arXiv:0707.4477v2 [astro-ph] 9 Aug 2007

Halo Star Streams in the Solar Neighborhood

Amanda A. Kepley

Department of Astronomy, Case Western Reserve University, Cleveland, OH 44106, U.S.A.; and Department of Astronomy, University of Wisconsin–Madison, 475 North Charter Street, Madison, WI 53706, U.S.A.

kepley@astro.wisc.edu

Heather L. Morrison

Department of Astronomy, Case Western Reserve University, Cleveland, OH 44106, U.S.A.

heather@vegemite.case.edu

Amina Helmi

Kapteyn Astronomical Institute, University of Groningen, P.O. Box 800, 9700 AV Groningen, Netherlands

ahelmi@astro.rug.nl

T.D. Kinman

National Optical Astronomy Observatory, P.O. Box 26732, Tucson AZ 85726, U.S.A.

tkinman@noao.edu

Jeffrey Van Duyne

Department of Astronomy, Yale University, P.O. Box 208121, New Haven, CT 06520, U.S.A.

vanduyne@astro.yale.edu

John C. Martin

University of Illinois at Springfield, 1 University Plaza, MS HSB 314, Springfield, IL 62703, U.S.A.

jmart5@uis.edu

Paul Harding

Department of Astronomy, Case Western Reserve University, Cleveland, OH 44106, U.S.A.

harding@dropbear.case.edu

John E. Norris and Kenneth C. Freeman

Research School of Astronomy and Astrophysics, Australian National University, Private Bag, Weston Creek PO, 2611 Canberra, ACT, Australia

jen@mso.anu.edu.au,kcf@mso.anu.edu.au

ABSTRACT

We have assembled a sample of halo stars in the solar neighborhood to look for halo substructure in velocity and angular momentum space. Our sample (231 stars) includes red giants, RR Lyrae variable stars, and red horizontal branch stars within 2.5 kpc of the Sun with [Fe/H] less than –1.0. It was chosen to include stars with accurate distances, space velocities, and metallicities as well as well-quantified errors. With our data set, we confirm the existence of the streams found by Helmi and coworkers, which we refer to as the H99 streams. These streams have a double-peaked velocity distribution in the z direction (out of the Galactic plane). We use the results of modeling of the H99 streams by Helmi and collaborators to test how one might use v_z velocity information and radial velocity information to detect kinematic substructure in the halo. We find that detecting the H99 streams with radial velocities alone would require a large sample (e.g., approximately 150 stars within 2 kpc of the Sun and within 20° of the Galactic poles). In addition, we use the velocity distribution of the H99 streams to estimate their age. From our model of the progenitor of the H99 streams, we determine that it was accreted between 6 and 9 Gyr ago. The H99 streams have [α/Fe] abundances similar to other halo stars in the solar neighborhood, suggesting that the gas that formed these stars were enriched mostly by Type II supernovae. We have also discovered in angular momentum space two other possible substructures, which we refer to as the retrograde and prograde outliers. The retrograde outliers are likely to be halo substructure, but the prograde outliers are most likely part of the smooth halo. The retrograde outliers have significant structure in the v_ϕ direction and show a range of [α/Fe], with two having low [α/Fe] for their [Fe/H]. The fraction of substructure stars in our sample is between 5% and 7%. The methods presented in this paper can be used to exploit the kinematic information present in future large databases like RAVE, SDSSII/SEGUE, and *Gaia*.

Subject headings: methods: statistical, Galaxy: halo, Galaxy: kinematics and dynamics, solar neighborhood

1. Introduction

The kinematics of stars in the Galaxy provide information about its structure and formation history. Early Galaxy formation models, most notably those by Eggen et al. (1962), postulated a monolithic collapse of gas and dust, with a large cloud of gas collapsing and forming stars. Later, Searle & Zinn (1978) suggested that the Galaxy was formed through a series of accretion events, with smaller proto-galaxies coming together to form a larger structure. Their scenario is more in keeping with our current understanding of how structures formed in the early universe in a "bottom-up" fashion (Steinmetz & Muller 1994; White & Springel 2000).

Ibata et al. (1994) discovered that the Galaxy is currently accreting the Sagittarius dwarf spheroidal galaxy. Stars from this system are not yet well-mixed with the rest of the Galactic halo either spatially or in velocity space. Could other halo accretion events be detected if the stars from the accreted object have become well-mixed with the stars in the halo spatially, but not in velocity or angular momentum space? Helmi et al. (1999, hereafter H99), found evidence in angular momentum space for streams in the solar neighborhood using a sample of 97 metal-deficient red giants and RR Lyrae stars within 1 kpc of the Sun and, using the sample properties, generated a model of the streams.

The purpose of this work is to search for further evidence for substructure in the local Galactic halo and to develop novel ways to detect halo substructure. In order to detect the subtle signs of kinematical substructure, accurate data are needed. We use two different halo star samples: the original H99 sample and a combined data set that includes local giants, red horizontal branch (RHB) stars, and RR Lyrae stars, all selected without kinematic bias. Both samples have full space velocities, distances, and metallicities. Further improvements to the solar neighborhood halo sample will be presented in the next paper in this series, H.L. Morrison et al. (2007, in preparation, hereafter M07), which will focus on the overall properties of the sample and their constraints on the formation history of the local halo, rather than specifically on substructure.

Full space velocities are difficult to obtain for many stars, preventing a complete analysis of their motions like that of H99. However, the H99 models and original data show structure even in their radial velocity distributions, especially when stars in a particular direction, e.g.

near the Galactic poles, are considered. In addition, other possible substructures that we discuss in this paper occupy the tails of the angular momentum distribution, and so may be detectable in radial velocities dominated by rotational velocity. Standard statistical tests such as the Shapiro-Wilk test for normality, which is quite sensitive to the behaviour of the tails of the distribution, can be used to detect such deviations. We use the H99 model of the streams as well as a model of a smooth halo to show how streams can be detected in one component of velocity (v_z), and we determine the detection limits for this method. We also extend this method to radial velocities for stars in the direction of the Galactic poles.

In recent years, increasingly large and precise data sets of abundances for multiple elements have made it possible to study a new dimension of substructure in the halo: the chemical patterns. Abundances trace the star formation history of the objects that became today's halo. A good general discussion of the possibilities of this technique is given in Freeman & Bland-Hawthorn (2002). In particular, the ratios of the α-elements such as Mg, Ca, and Ti to Fe allow the possibility of distinguishing between a chemical history where enrichment only comes from short-lived massive stars (Type II supernovae), and one where the contribution of Type Ia supernovae need to be considered as well. Type II supernovae preferentially enrich the interstellar medium (ISM) with α elements, while Type Ia supernovae produce more iron but need a longer period of chemical evolution. Thus the bulk of the local halo stars have a higher value of [α/Fe] than local disk stars, reflecting different formation conditions. However, there are some metal-poor stars that have unusually low values of [α/Fe], such as those in dwarf spheroidal galaxies (Shetrone et al. 2001, 2003; Tolstoy et al. 2003), a small number of outer halo globular clusters such as Pal 12 and Rup 106 (Brown et al. 1997, 1999), and some local halo field stars (Carney et al. 1997; King 1997; Nissen & Schuster 1997; Fulbright 2002; Stephens & Boesgaard 2002; Ivans et al. 2003; Venn et al. 2004). For stars from substructures identified via kinematic methods, we investigate whether there are any unusual patterns in [α/Fe].

Section 2 describes the compilation of the data sets used in this work in detail. Information about our model of the Galactic halo is given in Section 3 and our results are described and discussed in Section 4. Section 5 summarizes our conclusions.

2. Data Sets

The search for substructure in H99 is particularly powerful because estimates of all three space velocities are available for their sample. This allows the use of angular momentum (approximately conserved in a roughly spherical potential) to isolate stars with similar origins. In the pre-*Gaia* era, the need for three space velocities limits us to a relatively small

volume surrounding the Sun, where sufficiently accurate proper motions are available. It is important to note that methods of identifying satellite debris using physical quantities such as angular momentum and energy (e.g. Lynden-Bell & Lynden-Bell 1995; Helmi et al. 1999, 2006) rely strongly on good distance estimates. (The angular momentum estimate varies as distance squared, since two out of three velocity coordinates are obtained by multiplying the proper motion by the distance.) Thus the accuracy of distance estimates is very important.

2.1. H99 Data

The H99 sample stars were selected from the compilations of Beers & Sommer-Larsen (1995) and Chiba & Yoshii (1998, hereafter CY98) to have distances less than 1 kpc and [Fe/H] less than –1.6. This sample contains nearby stars in three evolutionary states: first ascent red giants, RHB stars, and RR Lyrae variable stars. These stars present different challenges for stellar population work. Good velocity estimates are difficult to obtain for RR Lyrae stars, but are relatively straightforward for red giants. This is because RR Lyrae stars show significant velocity variation due to pulsation, while first ascent giants and RHB stars have spectra that lend themselves readily to accurate velocity estimation. Conversely, distance estimates for RHB and RR Lyrae stars are good, but distance estimates for red giant stars less so. RR Lyrae and RHB stars show little variation in absolute magnitude with metallicity. For example, Martin & Morrison (1998) estimated a typical error of 10% for RR Lyrae distances, and Vivas et al. (2005) estimate 6%. First ascent red giants generally have less precise distances, because the position of the giant branch in the color-magnitude diagram depends strongly on metallicity, and so metallicity measurement errors propagate to a larger distance error of order 20% (see discussions in Morrison et al. 1990, 2003). The advantage of smaller distance errors for RHB stars is offset by the difficulty of identifying these stars; in order to separate the subtle differences in gravity between first ascent red giants below the horizontal branch and horizontal branch stars we need photometry from intermediate-band systems like Stromgren or DDO (Bond 1980; Norris et al. 1985; Anthony-Twarog & Twarog 1994). Luckily, many of the stars in the H99 sample were observed by Anthony-Twarog & Twarog (1994, hereafter ATT94) who obtained accurate Stromgren *uvby* colors, enabling them to classify stars as either RHB or first-ascent giants. Below we calculate the actual errors on distances, space velocities and angular momenta for the ATT stars, illustrating that these quantities are known remarkably precisely for a sample including red giants.

2.2. Combined Data Set

Since H99 was published there have been several improvements on the information available for the solar neighborhood giant and horizontal branch stars. In particular, Beers et al. (2000, B00 hereafter) presented a catalog of 2016 stars selected without kinematic bias, and we use preliminary results from a new sample of RR Lyraes with significantly improved radial velocity measurements (M07).

2.2.1. RR Lyrae Variables

While the Layden (1994) data set provided accurate [Fe/H] and distance measurements for the local RR Lyrae stars, the velocity measurements were less accurate (typical errors of 30 km s^{-1}). M07 obtained more accurate velocities for the RR Lyrae stars accessible from the north, observing most stars more than once and using high-quality light curves obtained by T.D. Kinman (1991, private communication) to correct for the large radial velocity amplitude of each star. Velocities were corrected for pulsation using the synthetic velocity curves of Liu (1991). Typical velocity errors are 15 km s^{-1}. Martin & Morrison (1998) published improved values of proper motion for RR Lyrae stars by averaging *Hipparcos* proper motions with accurate ground-based determinations from the USNO ACT reference catalog (Urban et al. 1998). We have selected a sample of 96 stars with [Fe/H] less than –1.0 from these data sets. Metallicities for these stars are from Layden (1994); Layden et al. (1996). The distances of stars in the M07 sample (derived using the Layden (1994) period-luminosity relation) range from about 0.5 kpc (RR Lyrae itself) to 2.5 kpc. Our sample presently only includes RR Lyrae stars of type ab.

2.2.2. Red giants and RHB Stars

We have selected a subset of the red giant stars in the B00 catalog for our expanded sample. In order to preserve the distance accuracy so important to the calculation of angular momentum, we critically compared the distance estimates given in the B00 catalog with those given by earlier work such as ATT94. This uncovered some surprisingly large, systematic differences in distance estimates.

Figure 1 shows that the B00 and ATT94 distances agree reasonably well for distances greater than 1 kpc. For distances less than 1 kpc, the ATT94 distances are on average a factor of 2 larger than the B00 distances, a remarkably large amount for local, well-studied stars.

Both papers use $B-V$ colors and the globular cluster giant branch parameterization of Norris et al. (1985) to estimate absolute magnitudes for the giant stars. B00 assumed that all giants are on the first-ascent giant branch, while ATT94 used the Stromgren $c1$ index to separate horizontal-branch and asymptotic giant branch (AGB) stars from first-ascent giants. AGB star contamination is expected to be small because of the short AGB lifetimes, but horizontal-branch stars are more common. Blueward of $(B-V)_0 \simeq 0.9$, we expect significant numbers of RHB stars to appear in the sample. Assuming that these stars were on the first ascent giant branch, as B00 did, will lead to significant underestimates of their distance. This error will become larger for the bluest stars. Figure 2 shows that this is indeed the case, with B00 distances being on average a factor of 2 smaller than the ATT94 distances for $(B-V)_0 = 0.6$.

Thus we have restricted our sample to giants from B00 with $(B-V)_0$ greater than 0.9, red giants and RHB stars from CY98 with distances determined by ATT94, and RR Lyrae stars from the M07 sample. We have also restricted the sample to stars with [Fe/H] less than –1.0 and distances less than 2.5 kpc, and eliminated stars with thick disk kinematics (see Section 4.3 for details). The $(B-V)_0$ criteria led us to accept 24 red giants and to reject 85 red giants from B00 that had otherwise acceptable distances and metallicities. Fourteen of the accepted stars were later eliminated from the final sample because of their thick disk kinematics (see Section 4.3). For stars in our sample within 0.5 kpc of the Sun, our distances agree with *Hipparcos* distances (ESA 1997) within the errors. The only exception is HD 135449, whose distance in Table 1 is twice the distance given by Hipparcos. In future versions of this sample (M07), we plan on using the Hipparcos distances for nearby stars. Metallicities in B00 come from a large variety of sources, but the ATT94 data (which dominate our combined sample of red giants and RHB stars) are significantly more homogeneous, being based either on *uvby* photometry (89 stars, an estimated [Fe/H] error 0.16 dex) or accurate spectroscopic abundances from the literature (68 stars).

2.2.3. Error Estimates

Because the data in our combined sample come from a variety of sources and include stars in different evolutionary stages, it is preferable to calculate the errors on derived quantities individually, since they can vary significantly (see Table 1 and Fig. 11). We propagated the known errors on distance, velocity, and proper motion through the calculation of v_R, v_ϕ, v_z, J_z, and $J_\perp$ using a Monte Carlo calculation, drawing new values of the input quantities from Gaussian distributions, recalculating the derived values and measuring the standard deviation of their distributions.

For the RR Lyrae and RHB stars, distance errors are relatively small, and have been assumed to be 7%. For the first ascent red giants in the sample, it is more difficult to quantify errors because the metallicity is the main driver of distance errors and many authors do not quote metallicity errors[1]. We have calculated distance errors individually for stars in the ATT94 sample (where accurate metallicity errors are given, and in fact a significant number of stars have multiple high-dispersion metallicity estimates) and for a small number of red giants, most of which are part of the outlier groups discussed in Section 4.3. To calculate distance errors, we used $B-V$ color and the globular cluster giant branch loci of Norris et al. (1985) with a Monte Carlo calculation of the effect of metallicity and color errors on the estimate of absolute magnitude.

For the five red giant stars not in the ATT94 sample, we made the following assumptions. Four (HD 18710, HD 174578, HD 214925 and CD –68 1881) have [Fe/H] values from Norris et al. (1985). Twarog & Anthony-Twarog (1994) have shown that the DDO [Fe/H] calibration used for these stars has systematic errors in some metallicity ranges. We have assigned [Fe/H] errors of 0.25, 0.50, 0.20 and 0.50 dex respectively to account for this. BD +30 2282 has metallicity from Hartkopf & Yoss (1982); we have assigned an [Fe/H] error of 0.35 dex for this star. There was also one giant in ATT94 (HD 128279) that was too blue to use the Norris et al. (1985) distance calibration for the Monte Carlo calculation. Luckily, it has a *Hipparcos* parallax of reasonable accuracy so we have simply used the parallax and its error rather than our other distance error estimation procedure.

2.2.4. Final Sample

We have error estimates for distances and derived quantities (velocities and angular momentum) for the great majority of the sample: 210 out of 231 stars. The combined sample has a median distance of 1.1 kpc, median distance error 7%, and median metallicity [Fe/H] = –1.7. Median errors on v_R, v_ϕ, v_z velocities are 15, 20 and 11 km s^{-1} respectively, making this sample well-suited for careful investigations of substructure.

Table 1 lists values of distances, metallicities, radial velocities, and galactocentric velocities for the red giants and RHB stars in the combined sample as well as the associated errors for these quantities. The RR Lyrae data will be published in M07. In Table 1, the radial velocities are heliocentric and the v_R, v_ϕ, and v_z velocities are relative to the cen-

[1]Note that CY98 calculated distance errors simply by assuming that the error on each metallicity value in their sample was 0.16 dex, while ATT94's actual quoted errors vary from 0.01 to 0.31 dex. We have set errors quoted at less than 0.1 dex to be 0.1 dex in our calculations.

ter of the Galaxy on a left-handed coordinate system. This has R pointing away from the center, ϕ increasing in the direction of Galactic rotation, and z pointing towards the north Galactic pole (NGP). Note that our angular momenta are calculated on this left-handed system in order to directly compare our results with the results of H99. (See the Appendix for more details.) The velocities were corrected for the motion of the Sun and LSR using $v_{lsr} = 220.0$ km s^{-1}, $U_\odot = -9.0$ km s^{-1}, $V_\odot = 12.0$ km s^{-1}, and $W_\odot = 7.0$ km s^{-1} on the standard left-handed coordinate system (Blaauw & Schmidt 1965; Mihalas & Binney 1981). The Sun was assumed to be 8.0 kpc from the Galactic center. See the Appendix for the transformation between the local, Sun-centered coordinate system and the galactocentric coordinate system.

The sample was selected without kinematic bias, but is spatially incomplete: it has fewer stars with low $|b|$ because of the difficulty of identifying these rare halo stars in heavily reddened regions. We show the distribution of distance and $|b|$ in Figure 3. It can be seen that the RR Lyrae sample is more complete in $|b|$ than the giant sample, although neither are fully complete in $|b|$. The giant sample has a lower mean distance than the RR Lyrae sample because of the intrinsic rarity of the RR Lyrae stars. Since all three velocity components can be measured for each star, the spatial incompleteness does not cause a bias in the velocity distribution directly. However, the bias toward high Galactic latitude does select against stars with a flattened space distribution, such as the metal-poor stars in the thick disk (Norris et al. 1985; Morrison et al. 1990). Therefore, we would expect any such stars to be under-represented in our sample.

Since there will be a significant number of binaries in any sample of stars (for example, 17% in the sample of metal-poor giants of Carney et al. 2003), we need to consider the effect of binarity on our estimates of distance and velocity. Fortunately, because our sample is composed of giants and horizontal branch stars, the effect of any undetected binaries on the distance estimates will be small. Carney et al. (2003) studied 91 metal-poor red giants and RHB stars, (68 in common with our sample) and identified 8 spectroscopic binaries. The median velocity amplitude of these binaries is 8 km s^{-1}, which is small compared to our typical error on a U,V or W velocity (10-15 km s^{-1}). While we expect a similar number of undetected spectroscopic binaries in our sample, the effect on our conclusions will be negligible. Similarly, the "velocity jitter" that is seen in some stars close to the giant branch tip is of an even smaller magnitude (of order 5 km s^{-1}) and will not affect our conclusions either.

3. Model Information

Helmi & White (1999) described models used to study the disruption of satellite galaxies by the Milky Way. H99 used these to model the progenitor of the star streams they detected in the solar neighborhood. The remnants of a progenitor with an initial velocity dispersion of 18 km s^{-1} and core radius of 0.5-0.65 kpc fit the star streams discovered in H99. Its orbit has an apocenter at 16 kpc, pericenter at 7 kpc, a maximum height above the plane of 13 kpc, and a radial period of 0.4 Gyr. The present paper uses an improved version of the model, which better accounts for the self-gravity of the satellite and has positions and space velocities for 10^6 particles in the disrupted progenitor from 0 Gyr-13 Gyr. After 3-5 Gyr, these particles fill much of the space between 7 and 16 kpc from the Galactic center (the amount of debris from the progenitor peaks at the solar circle) and are very well-mixed spatially within ∼5 kpc from the Sun. The disrupted progenitor still has some structure in velocity and angular momentum space, however, as can be seen in Figure 4.

In addition, we have created a model of a smooth halo. This model allows us to test the null hypothesis that the halo has no substructure. The density distribution of the smooth halo (number of stars per unit volume) is proportional to $r^{-3.5}$ (Zinn 1985; Vivas & Zinn 2006). The velocity distribution of the halo was modeled using a velocity ellipsoid (Schwarzschild 1907). The models were created by randomly selecting points from these distributions. Figure 5 shows one realization of this model in velocity and angular momentum space. The parameters $\langle v_R \rangle$, $\langle v_\phi \rangle$, $\langle v_z \rangle$, σ_R, σ_ϕ, and σ_z were determined by finding the average and the standard deviation of the v_R, v_ϕ, and v_z velocity distributions from the combined data set excluding known stream stars.

The standard velocity ellipsoid numbers for the halo (e.g. Chiba & Beers 2000) were not used because the H99 star streams, in particular, bias the velocity distributions. For example, Figure 6 shows that the stream stars have large absolute z velocities. Including these stars in the velocity ellipsoid calculations changes σ_z from 84 km s^{-1} to 101 km s^{-1}. Table 2 gives the derived velocity ellipsoid parameters for our combined sample (stars with distances less than 2.5 kpc and [Fe/H] ≤ -1.0, excluding likely thick disk stars), both with and without stream stars. In the case of $\langle v_R \rangle$ and $\langle v_z \rangle$, the parameters used are consistent with zero within the errors. However, $\langle v_\phi \rangle$ is not consistent with zero. Chiba & Beers (2000) find a similar $\langle v_\phi \rangle$ for their sample within 1 kpc of the Sun and note that $\langle v_\phi \rangle$ decreases when larger distance ranges are included. Note that excluding the star streams from the sample used to determine the velocity ellipsoid also increases the anisotropy of the halo.

4. Identifying Structure in the Tails of the Velocity Distribution

4.1. Method

Using distances and full space velocities of metal-poor red giants and RR Lyrae stars, H99 identified the remnant of a merger between a small satellite galaxy and the Milky Way. Since obtaining proper motions of stars is difficult, another way to identify subtle merger remnants is desirable. Here we explore signatures visible in the tails of the velocity distribution. Figure 6 plots the H99 data in velocity and angular momentum space. Its bottom panel plots J_z, the component of the angular momentum (per unit mass) out the plane of the Galaxy's disk, versus $J_\perp = \sqrt{J_x^2 + J_y^2}$, the angular momentum (per unit mass) in the plane of the disk. The H99 stream stars (*large circles*) clearly occupy a different region of phase space than the rest of the halo stars, attesting to the debris' common origin as a Galactic satellite. Figure 6 (*top panels*) shows cylindrical velocity coordinates. The stream stars (*large circles*) are located in two clumps, one with $v_z \sim -200$ km s^{-1} and the other with $v_z \sim 200$ km s^{-1}. The bimodality in v_z seen for the nearby stream stars comes about because their orbits reach to a large distance (13 kpc) above and below the Galactic plane. Therefore, any nearby substructure stars will be passing through with high positive or negative v_z values. We can anticipate that this bimodality will be less marked as more distant stars are included in the sample, because it will include stream stars with smaller values of $|v_z|$.

Note that the v_z components of the H99 streams extend well into the tails of the velocity distribution, as can be seen in Figure 7. A smooth halo velocity distribution is well-approximated as a multi-dimensional normal (Gaussian) distribution (e.g. Binney & Merrifield 1998), so testing the v_z distribution for normality may reveal the presence of substructure like that in H99. In addition, the line of sight component of velocity for stars near the Galactic poles is dominated by the v_z component of the star's velocity. Therefore, if one uses a sample of stars near the Galactic poles, one should be able to test for structure in the v_z distribution using only radial velocities. While with this technique we are only able to identify the presence of substructure in the data, not necessarily the substructure itself, it will be useful in identifying data sets where other observers might want to aggressively pursue proper motions and distances.[2]

[2]One might imagine employing a genetic-algorithm technique to find stream stars where random groups of stars are selected, the Shapiro-Wilk product calculated, and the groups that have the highest p-values are bred together to create the next generation of groups to test. This is, of course, a computationally intensive method.

There are many tests for deviations from normality; one of the most powerful is the Shapiro-Wilk test (Shapiro & Wilk 1965; D'Agostino 1986). This test is based on the concept of probability plots, which plot the cumulative distribution function[3] using a transformation of the vertical axis that makes normally distributed data fall along a straight line. Examples of probability plots are shown in Chapter 1 of D'Agostino & Stephens (1986). The slope of this line gives an estimate of σ for a normal distribution. The Shapiro-Wilk test compares this slope with the sample standard deviation (Stephens 1986). This technique is particularly sensitive to deviations from normality in the tails of the distribution. Code for this test (Royston 1995) can be obtained at StatLib.[4]

To test this method, we applied the Shapiro-Wilk test to the H99 v_z data. Here the null hypothesis is that the data have a normal v_z distribution, and the probability value (p-value for short) indicates how often data with a normal distribution would produce this data set. Thus the smaller the p-value, the less likely it is that the data come from a normal distribution. (Note, however, that a high p-value does not mean that the sample distribution is normal, just that it is consistent with a normal distribution.) The results of this test are given in Table 3. We list the tested data set and the associated p-value. The entire sample fails the Shapiro-Wilk test at the 1% level. When the H99 stream stars and one other star (HD 124358) at ($J_z \sim -1500$, $J_\perp \sim 2300$) are excluded, however, the sample passes the Shapiro-Wilk test. The additional excluded star, indicated by a large triangle, has a very retrograde orbit and is well away from the rest of the data in angular momentum space; it may belong to another stream (see Section 4.3). These results demonstrate the effectiveness of this method for detecting streams like those in H99, where the stars occupy the tails of one component of the velocity distribution.

4.2. Modeling Stream Detections with Distance

Having established that we are able to detect substructure using the v_z velocity distribution, now we use the H99 model of the debris and our model of the smooth halo to see (1) how changing the sample distance limit affects our ability to detect streams and (2) how close stars need to be to the Galactic pole to detect substructure using radial velocity information only.

To characterize stream detections, we produced random samples with sizes ranging from

[3]The cumulative distribution function gives the fraction of data points that are less than or equal to a value as a function of value: $CDF(x) = P(X \leq x)$, where x is the value and X is the data.

[4]http://lib.stat.cmu.edu/apstat/R94

20 to 4000 stars, and distance limits of 1, 2, 3, 4 and 5 kpc. In each case, we produced 10,000 different realizations of the sample. While the stream stars are spatially well-mixed up to 5 kpc from the Sun, the relative number of stream stars to smooth halo stars drops slowly as we move away from the Sun; see Figure 8. The number of stream stars in each distance-limited sample was scaled using the models so that stream stars made up 10% of the sample for a distance limit of 1.0 kpc. The maximum distance limit in our simulations was 5 kpc, since the velocity ellipsoid of the halo may change beyond this distance (e.g. Vedel & Sommer-Larsen 1990). For each sample, we tested the v_z distribution for normality using the Shapiro-Wilk test. We calculated the p-value (significance level) for each of the 10,000 realizations of the sample, and then calculated the average p-value for each sample.

Figure 9 shows the average p-value as a function of sample size for various distance limits in our v_z samples. P-values below 5% fail the Shapiro-Wilk test for normality. The number of stars needed to detect the stream with a 1.0 kpc distance limit is less than the sample size of H99 sample with this distance limit (101 stars), so it is unsurprising that we were able to detect the H99 streams using this method (see Table 8). As the distance limit increases, more stars are needed in the sample to detect the presence of the H99 streams. For example, with a distance limit of 5 kpc, approximately 600 stars are needed to detect the H99 streams, but only 75 stars are needed with a distance limit of 1.0 kpc. There are two causes here. First, the fraction of stream stars in a sample decreases slowly as the sample distance limit increases (see Fig. 8). Second, the velocity distribution of the stream changes away from the solar neighborhood, and this results in fewer stream stars with extreme values of v_z. (Since the high-energy debris from the progenitor is bound to the Galaxy, stars nearest the plane will have the largest v_z velocities. As the distance from the plane increases, the v_z velocities of the stars will decrease.) The result of both effects means that increasing the distance limit on a sample does not necessarily increase the detection probability, if it does not have enough stars for the stream to be detected in the sample with the larger distance limits.

To use radial velocities to identify kinematic structure in v_z, we need to identify how close the sample stars need to be to the Galactic poles to have enough v_z velocity information to detect structure. To examine this, we generated five different distance limited samples ($D \leq 1.0$, $D \leq 2.0$, $D \leq 3.0$, $D \leq 4.0$, and $D \leq 5.0$ kpc) and applied four different Galactic latitude limits to each sample ($|b| \geq 40$, $|b| \geq 50$, $|b| \geq 60$, $|b| \geq 70$, and $|b| \geq 80$). The stream stars were assumed to be well mixed spatially so we used the same normalization for the stream stars as in the previous set of simulations. We calculated the radial velocity of each star in each sample and then used the same algorithm as above substituting the radial velocities for the v_z velocities to determine an average p-value for the radial velocity distribution of a sample. The results of these simulations are given in Figure 10.

Comparing Figures 9 and 10, one sees that for lower Galactic latitude limits, much larger sample sizes are needed to detect streams. As the Galactic latitude limits get further from the Galactic pole, the width of the smooth halo radial velocity distribution increases, drowning out the presence of stream stars in the wings of the distribution. As we sample closer to the Galactic poles, the sample size needed to detect the H99 streams using radial velocities approaches that needed to detect the streams in v_z velocity space. In short, using the radial velocity test to overcome a lack of proper motion data requires a significant increase in the sample size.

4.3. Streams in the Combined Data Set

We used the combined sample described in Section 2.2 to investigate further the applicability of the Shapiro-Wilk test to real data. We concentrate here on looking for outliers in the J_z versus $J_\perp$ distribution. In future work (M07), we will investigate structure within the J_z versus $J_\perp$ distribution, i.e., within the angular momentum distribution of the disk and the halo themselves, such as in Navarro et al. (2004).

While H99 used two different distance limits in their analysis (1 and 2.5 kpc) in order to limit the effect of larger errors in tangential velocity, our direct calculation of errors on the angular momenta make this unnecessary. H99 also limited their sample to stars with [Fe/H] ≤ -1.6 to exclude thick disk stars. We chose simply to exclude such stars using their position on the angular momentum plot. To be considered a thick disk star, the star needed to have a J_z between 1500 and 2500 kpc km s^{-1} and a $J_\perp$ less than 600 kpc km s^{-1}. These limits were chosen to match the angular momentum distribution of stars in the Nordström et al. (2004) sample with [Fe/H] greater than –1.0 and heliocentric distances less than 2.5 kpc. In addition, the star's v_ϕ needed to be near 220 km s^{-1} with all other velocity components near zero. Note that a star traveling at the speed (220 km s^{-1}) and position (8.0 kpc) of the LSR has a J_z of 1760 kpc km s^{-1}. The $J_\perp$ limit reflects the velocity dispersion of stars in the disk. These criteria excluded 24 stars, of which seven had [Fe/H] < -1.6. Note the symmetry about $J_z \sim 0$ for the resulting halo distribution (Fig. 11). The clumpiness within the distribution of halo stars will be investigated in M07.

We have identified the H99 stream stars and two other groups of outliers in the combined sample. The properties of the H99 stream stars and the outliers are given in Tables 4, 5, and 6. Figure 11 shows where these stars fall on the angular momentum and cylindrical velocity plot. The H99 streams are clumped in angular momentum and cylindrical velocity space, but not in Galactic coordinates. The first group of outliers, on the retrograde (left) side of the angular momentum plot, might also be tidal debris. It has extent and isolation similar

to the H99 streams. It also forms a kinematically distinct group in the cylindrical velocity plots (at $\langle v_\phi \rangle \sim -300$ km s^{-1}) as well as being completely made up of low metallicity stars (see Table 5; Venn et al. (2004) have already noted the chemical homogeneity of the extreme retrograde stars in the solar neighborhood). It is not, however, as tightly clumped in velocity space as the H99 streams. The second group of outliers is located on the prograde (lower right) side of the angular momentum plot and has kinematics similar to disk stars, but with higher J$_z$ ($\langle v_\phi \rangle \sim 300$ km s^{-1}, $\langle v_R \rangle \sim 0$ km s^{-1}, $\langle v_z \rangle \sim 0$ km s^{-1}). The prograde outlier group is also very metal poor (see Table 6). Because of the closeness to the disk and thick disk region of the angular momentum plot, it is possible that this group is related to the disk or was accreted into the disk by dynamical friction as in Abadi et al. (2003).

We can estimate the probability of stars from a smooth halo populating the above regions in angular momentum space using the smooth halo model described in Section 3. We randomly selected 231 stars within 2.5 kpc of the Sun from this model and counted the number of stars in each region of the angular momentum plot where we see outliers in the data. The size of the angular momentum region was chosen to be large enough to enclose all the outliers and their errors. We did not include AS Cnc in the H99 streams region because we are not sure if it is really part of this group. (See Section 4.3.1.) We also randomly generated errors for the points from the model based on the distribution of errors in the combined data set. The errors were modeled as normal distributions with mean zero, $\sigma(J_z) = 186$ kpc km s^{-1}, and $\sigma(J_\perp) = 107$ kpc km s^{-1}. This process was repeated for 100,000 trials. Table 7 gives the box parameters, the probability that there would be as many or more stars as there are possible stream stars in the box if the halo was entirely smooth, and the average number of stars in the each region for a smooth halo.

For the H99 stream, we found that there was a very low probability of having 11 smooth halo stars in that region of the angular momentum diagram. This result supports the conclusions of H99. In the retrograde outlier region, there is a 7% chance of having six or more stars in that region of the angular momentum diagram. This set of outliers is possibly another stream. The simulations tell a different story for the prograde outliers. The probability for having at least three stars in this region of the angular momentum diagram is 70%. In addition, changing the criterion used to exclude thick disk stars could eliminate the prograde group or fill in the region between the halo distribution and the prograde group. The prograde outliers are likely smooth halo stars (perhaps with some contribution from the thick disk as well) rather than part of a stream.

4.3.1. H99 Stream Properties

The H99 streams make up 5% of our total sample. For a subsample of the combined data set with the same parameters as the H99 sample ([Fe/H] ≤ -1.0 and distances less than 1.0 kpc), the fraction is 9%. We detect 11 of 12 stars that H99 detected and possibly add one more star to the streams (AS Cnc). The missing H99 star (HD 214925) we group with the retrograde outlier group rather than the H99 streams. In Figure 11, AS Cnc is located very far from the rest of the H99 group in angular momentum space (at $J_z \sim 4000$ kpc km s^{-1} and $J_\perp \sim 3600$ kpc km s^{-1}) , but agrees with the rest of the stars in velocity space. Therefore, we cannot say for certain whether AS Cnc is part of the H99 group without better data on its distance and space velocities. We include AS Cnc in our list of members of the H99 streams for completeness, not because we are certain it is a member.

Pilachowski et al. (1996) and Fulbright (2000, 2002) gave high-dispersion abundance analyses for three of the H99 stream stars in Table 4: HD 128279, BD+30 2611 and HD 175305. Their [Mg/Fe] and [α/Fe] abundances are similar to other halo stars in the solar neighborhood, suggesting that the gas that formed these stars was enriched mostly by Type II supernovae.

Fiorentin et al. (2005) has performed a similar analysis to ours using only the B00 data and finds seven additional stars in the H99 streams. Two of the Fiorentin et al. (2005) stars (HD 214161 and BPS CS 22189-0007) we excluded from our sample because they were classified by B00 as giants and had $(B-V)_0$ less than 0.9; they are likely to have underestimated distances (see Section 2.2.2). Fiorentin et al. (2005) also include RZ Cep in their list of members of the H99 streams. RZ Cep is a type c RR Lyrae and thus not included in the M07 sample of RR Lyrae stars; it could be an additional member of the stream. Finally, five of the stars that Fiorentin et al. (2005) detect (BPS CS 22948-0093, BPS CS 30339-0037, BPS CS 29513-0031, BPS CS 29504-0044, and BPS CS 22876-0040) are classified by B00 as turnoff stars. We did not include these stars in our sample because the distance estimates used in B00 for turnoff stars were based on UBV-photometry and thus not able to deal with the evolution of turnoff stars up to the subgiant branch. This ambiguity introduces additional uncertainty into the distance estimates for these stars (Schuster et al. 2004, especially their Fig. 8).

We tested the v_z velocity data for normality using the Shapiro-Wilk test. The results of these tests are given in Table 8. When the H99 stream stars are excluded from the sample, it tests positive for normality. Comparing our results to the simulations in Section 4.2, it is not surprising that we were able to detect the H99 streams in this sample using only v_z velocities. We did not test the radial velocity distribution of this sample for normality because there are not enough stars in the sample for this test to detect structure.

We can use the observed asymmetry in the v_z velocity distribution of the H99 streams along with our model of them to estimate the how long ago the progenitor was accreted. Initially, all stars are bound, and as time goes by, the stars are released leading to the formation of streams. These streams will phase-mix, and after many gigayears, this mixing will have progressed so that half the stars will cross the Galactic disk in each direction. In Figure 11, we see that the observed fraction of stars in the stream with negative v_z is 0.72 (8/11). To estimate the age of the H99 streams, we selected 11 model stars within 2.5 kpc of the Sun from our simulation and determined the fraction in the stream with negative v_z. We repeated this 1000 times to build up a probability distribution. We then compared the observed fraction of stars (8/11 = 0.72) to this probability distribution to determine an age (Fig. 12). We find that the observed fraction is matched by the mean simulated fraction for a progenitor that was accreted between 6 and 9 Gyr ago. Although we cannot determine a definite age, we can rule out the possibility that the stream is either very young (3 Gyr) or very old (12 Gyr). Future observations can improve this situation. By increasing the observed total number of stars in the streams, the width of the peak of the probability distribution in Figure 12 decreases allowing a more accurate determination of the age of the accretion event.

4.3.2. Retrograde Outlier Properties

The retrograde outliers do not add significant structure to the v_z velocity distribution (the sample passes the Shapiro-Wilk test if the H99 streams, but not the retrograde outliers, are removed), but they do have significant structure in the v_ϕ direction, as can be seen in Figure 11. To see if the Shapiro-Wilk test is able to pick out these deviations from normality, we ran various samples of v_ϕ data through the Shapiro-Wilk test. The results are shown in Table 9. Excluding the retrograde group of stars (Fig. 11, *inverted triangles*) causes the sample to pass the Shapiro-Wilk test (test positive for normality). Indeed, all the samples that pass the Shapiro-Wilk test exclude this group of stars, which are very far from the rest of the v_ϕ velocities. Samples excluding only the prograde outliers do not test positive for normality. Evidently removing the prograde outliers from the sample just removes stars from the tail of the normal distribution of the halo and does not remove substructure.

We note that this group of stars has an extremely low value of J_z. The 38 globular clusters with proper motion estimates summarized by Dinescu et al. (1999), most of which are within 10 kpc of the Galactic center, have J_z values ranging from –664 to 2307 kpc km s^{-1}, while the mean value of J_z for our retrograde group is –2500 kpc km s^{-1}. However, larger samples of nearby proper-motion selected stars have produced stars with even more extreme

negative velocities, for example Kapteyn's star group, which has a mean J_z around –4000 kpc km s^{-1} (Eggen 1996).

Three of the stars from the retrograde substructure also have high-dispersion abundance information from Pilachowski et al. (1996), McWilliam et al. (1995), and Gratton & Sneden (1988): HD 6755, HD 200654 and CD–24 1782. Interestingly, these stars show a range of [α/Fe]: one has roughly normal [α/Fe] for the local halo while the other two have low [α/Fe] for their [Fe/H]. Note that our retrograde group corresponds roughly to the "extreme retrograde" class of Venn et al. (2004), and we find a similar behavior (somewhat lower [α/Fe] than normal) with our improved kinematical measures.

4.3.3. Discussion

Including both the H99 streams and the retrograde outliers gives a substructure fraction of 7% for the halo. The fraction of stream stars in the local halo is therefore at least 5% and possibly as high as 7% in this sample. Gould (2003) produced an estimate of the overall amount of substructure in the local halo (its "granularity") using an updated version on the NLTT proper motion sample. This method uses the fact that dominant streams in the solar neighborhood will not show spatial substructure over such a small volume, but will produce correlations between different components of velocity (non-zero cross terms in the velocity dispersion tensor). These will be reflected in the proper motion distribution. The fraction of stream stars in our sample is consistent with the upper limit set in Gould (2003), that one stream can comprise no more than 5% of the halo.

Chiba and Beers (2000) noted that when they increase the sample size of halo stars to 3 times that of H99 (728 stars), they only find nine stream stars total. There are several reasons why they may not have found more stream stars. First, the box that they use in their Figure 15 to identify the stream is too small. Our Figure 4 shows the distribution of stars in the model within 2.5 kpc in angular momentum and velocity space. This distribution is much larger than the box that Chiba and Beers (2000) selects. They also do not remove stars with thick disk kinematics ($J_z \sim 1750$ kpc km^{-1} and $J_\perp \sim 0$ kpc km^{-1}) from their sample, thus decreasing the percentage of H99 stream stars. Note, however, that the clumps in the $v_\phi - v_z$ velocity space are still apparent in their diagram, so it is still possible to pick out the H99 streams in their larger sample. This example illustrates the need to look not only at a angular momentum plot, but also a velocity plot to confirm membership in a moving group.

5. Conclusions

We have assembled a sample of halo stars in the solar neighborhood to look for substructure in velocity and angular momentum space. Our sample of 231 stars includes red giants, RR Lyrae variable stars, and RHB stars within 2.5 kpc of the Sun with [Fe/H] less than –1.0. It was chosen to include stars with well-quantified errors and accurate distances, space velocities, and metallicities. Understanding the errors in the measured and derived quantities, especially distance, is crucial for this work since they may distort any underlying substructure.

With our data set, we confirm the existence of the streams found by H99, which we refer to as the H99 streams. These streams have significant structure in their velocity distribution in the z direction (out of the Galactic plane). We use the results of H99 to test how one might use v_z velocity information and radial velocity information to detect kinematic substructure in the halo. We find that detecting the H99 streams with radial velocities alone would require a large sample (e.g., approximately 150 stars within 2 kpc of the Sun and within 20° of the Galactic poles). We also use the structure in the velocity distribution of the H99 streams to estimate the age of this group. From our model of the H99 progenitor, we determine that the H99 streams' progenitor was accreted between 6 and 9 Gyr ago.

We have also discovered, in angular momentum space, two other possible substructures, which we refer to as the retrograde and prograde outliers. For the retrograde outliers, there is a low probability of that region of the angular momentum diagram being occupied by six or more smooth halo stars. Based on this evidence, the retrograde outliers are likely members of a stream. The prograde outliers, however, are most likely smooth halo stars (perhaps with some contribution from the thick disk as well) rather than part of a stream. The retrograde outliers display significant structure in the v_ϕ direction. Samples excluding the retrograde outliers pass our test for normality in the v_ϕ direction. The fraction of stars in our sample that are stream stars is between 5% and 7%.

For H99 streams, the [Mg/Fe] and [α/Fe] abundances are similar to other halo stars in the solar neighborhood, suggesting that the gas that formed these stars was enriched mostly by Type II supernovae. The retrograde outliers show a range of [α/Fe]: one has roughly normal [α/Fe] for the local halo while the other two have low [α/Fe] for their [Fe/H]. Note that our retrograde group corresponds roughly to the "extreme retrograde" class of Venn et al. (2004), and we find a similar behavior (somewhat lower [α/Fe] than normal) with our improved kinematical measures.

Although we are not the first to note that stellar debris from the disruption of a satellite would have a double-peaked distribution in galactocentric radial velocity (see also Meza et al.

2005), the methods developed in this paper add to the toolbox of kinematic methods (e.g. H99 Helmi et al. 2006) being developed to exploit future large databases such as RAVE (Steinmetz et al. 2006), SDSSII/SEGUE (Beers et al. 2004), and *Gaia* (Turon et al. 2005) to detect kinematic substructure in our Galaxy's halo. These tools, in conjunction with studies of spatial over-densities in the Milky Way (e.g. Willman et al. 2002; Belokurov et al. 2006), will provide crucial answers to the puzzle of how our Galaxy was formed.

A. A. K. was supported by a NSF Graduate Research Fellowship during portions of this work. H. L. M. acknowledges the support of NSF grant AST-0098435. A. A. K. would like to thank Eric M. Wilcots for his patience while she finished this paper, and H. L. M. thanks Bruce Twarog and Barbara Anthony-Twarog for their helpful explanations of the *uvby* luminosity classifications and Kim Venn for a useful discussion on [α/Fe] measurements. The authors would also like to thank the referee for his or her helpful comments. We made extensive use of the SIMBAD astronomical database for this project.

A. Transforming Local Heliocentric Coordinates to Galactocentric Model Coordinates

Given the wide variety of coordinate systems used in Galactic astronomy, we explicitly derive the transformation between the local, Sun-centered coordinate systems (x', y', z') used in this paper and the Galactocentric coordinate system used in the H99 models (x, y, z). Figure 13 illustrates the two coordinate systems. The local velocity coordinate system is a left-handed coordinate system with the x' axis pointing away from the Galactic center, the y' axis pointing in the direction of Galactic rotation, and the z' axis pointing in the direction of the NGP. Note that the $L_{z'}$ angular momentum vector points in the direction opposite of the z' axis. In other words, the Galaxy rotates clockwise when you look down from the NGP. The model coordinate system used in H99 is also left-handed.

The position of a star with respect to the Sun is given by

$$x' = -d\cos(b)\cos(l) \quad \text{(A1)}$$

$$y' = d\cos(b)\sin(l) \quad \text{(A2)}$$

$$z' = d\sin(b) \quad \text{(A3)}$$

where d is the distance to the star in kpc, b is the Galactic latitude, and l is the Galactic longitude. The Galactocentric model coordinates are then

$$x = 8.0 \text{ kpc} + x' \quad \text{(A4)}$$

$$y = y' \quad \text{(A5)}$$
$$z = z' \quad \text{(A6)}$$

where 8.0 kpc is the distance between the Sun and the Galactic center.

To transform the observed space velocities to the Local Standard of Rest (LSR) frame, we use the equations

$$v_{x'} = U + u_\odot \quad \text{(A7)}$$
$$v_{y'} = V + v_\odot + v_{lsr} \quad \text{(A8)}$$
$$v_{z'} = W + w_\odot \quad \text{(A9)}$$

where U, V, and W are the space velocities directed toward the Galactic anti-center, toward the direction of rotation, and toward the NGP. We used the values $v_{lsr} = 220.0$ km s^{-1}, $u_\odot = -9.0$ km s^{-1}, $v_\odot = 12.0$ km s^{-1}, and $w_\odot = 7.0$ km s^{-1} (Blaauw & Schmidt 1965; Mihalas & Binney 1981) to correct for the motions of the Sun and the LSR. These velocities are the velocities in the model frame, i.e., the following

$$v_x = v_{x'} \quad \text{(A10)}$$
$$v_y = v_{y'} \quad \text{(A11)}$$
$$v_z = v_{z'}. \quad \text{(A12)}$$

The angular momentum components (per unit mass) are then the cross products

$$J_x = yv_z - v_y z \quad \text{(A13)}$$
$$J_y = zv_x - v_z x \quad \text{(A14)}$$
$$J_z = xv_y - v_x y \quad \text{(A15)}$$

and $J_\perp$ is $\sqrt{J_x^2 + J_y^2}$. Note that these angular momentum products are calculated on a left-handed system. While this does not make a difference in $J_\perp$, a left-handed J_z points in the opposite direction as a right-handed J_z. In other words, the left-handed J_z of a star near the Sun is 220 km s^{-1} $\times$ 8 kpc = 1760 kpc km s^{-1}, while the traditional right-handed J_z of a star near the Sun is -1760 kpc km s^{-1}.

REFERENCES

Abadi, M. G., Navarro, J. F., Steinmetz, M., & Eke, V. R. 2003, ApJ, 597, 21

Anthony-Twarog, B. J. & Twarog, B. A. 1994, AJ, 107, 1577

Beers, T. C., Allende Prieto, C., Wilhelm, R., Yanny, B., & Newberg, H. 2004, Publ. Astron. Soc. Australia, 21, 207

Beers, T. C., Chiba, M., Yoshii, Y., Platais, I., Hanson, R. B., Fuchs, B., & Rossi, S. 2000, AJ, 119, 2866

Beers, T. C. & Sommer-Larsen, J. 1995, ApJS, 96, 175

Belokurov, V., et al. 2006, ApJ, 642, L137

Binney, J. & Merrifield, M. 1998, Galactic Astronomy, (3rd ed.; Princeton, N.J.: Princeton University Press)

Blaauw, A. and Schmidt, M. 1965, *Galactic Structure*, (Chicago, University of Chicago Press).

Bond, H. E. 1980, ApJS, 44, 517

Brown, J. A., Wallerstein, G., & Gonzalez, G. 1999, AJ, 118, 1245

Brown, J. A., Wallerstein, G., & Zucker, D. 1997, AJ, 114, 180

Carney, B. W., Wright, J. S., Sneden, C., Laird, J. B., Aguilar, L. A., & Latham, D. W. 1997, AJ, 114, 363

Carney, B. W., Latham, D. W., Stefanik, R. P., Laird, J. B., & Morse, J. A. 2003, AJ, 125, 293

Chiba, M. & Beers, T. C. 2000, AJ, 119, 2843

Chiba, M. & Yoshii, Y. 1998, AJ, 115, 168

D'Agostino, R. B. 1986, in Goodness-of-Fit Techniques. ed. R. B. D'Agostino & M. A. Stephens (New York: Dekker), 367

D'Agostino, R. & Stephens, M., eds. 1986. Goodness-of-Fit Techniques. New York: Marcel Dekker, Inc.

Dinescu, D. I., Girard, T. M., & van Altena, W. F. 1999, AJ, 117, 1792

Eggen, O. J. 1996, AJ, 112, 1595

Eggen, O. J., Lynden-Bell, D., & Sandage, A. R. 1962, ApJ, 136, 748

ESA 1997, VizieR Online Data Catalog, 1239, 0

Fiorentin, P. R., Helmi, A., Lattanzi, M. G., & Spagna, A. 2005, A&A, 439, 551

Freeman, K., & Bland-Hawthorn, J. 2002, ARA&A, 40, 487

Fulbright, J. P. 2000, AJ, 120, 1841

Fulbright, J. P. 2002, AJ, 123, 404

Gould, A. 2003, ApJ, 592, L63

Gratton, R. G., & Sneden, C. 1988, A&A, 204, 193

Hanson, R. B., Sneden, C., Kraft, R. P., & Fulbright, J. 1998, AJ, 116, 1286

Hartkopf, W. I., & Yoss, K. M. 1982, AJ, 87, 1679

Helmi, A., Navarro, J. F., Nordström, B., Holmberg, J., Abadi, M. G., & Steinmetz, M. 2006, MNRAS, 365, 1309

Helmi, A. & White, S. D. M. 1999, MNRAS, 307, 495

Helmi, A., White, S. D. M., de Zeeuw, P. T., & Zhao, H. 1999, Nature, 402, 53

Ibata, R. A., Gilmore, G., & Irwin, M. J. 1994, Nature, 370, 194

Ivans, I. I., Sneden, C., James, C. R., Preston, G. W., Fulbright, J. P., Höflich, P. A., Carney, B. W., & Wheeler, J. C. 2003, ApJ, 592, 906

King, J. R. 1997, AJ, 113, 2302

Layden, A. C. 1994, AJ, 108, 1016

Layden, A. C., Hanson, R. B., Hawley, S. S., Klemola, A. R., & Hanley, C. J. 1996, AJ, 112, 2110

Liu, T. 1991, PASP, 103, 205

Lynden-Bell, D., & Lynden-Bell, R. M. 1995, MNRAS, 275, 429

McWilliam, A., Preston, G. W., Sneden, C., & Searle, L. 1995, AJ, 109, 2757

Martin, J.C., & Morrison, H.L. 1998, AJ, 116, 1724

Meza, A., Navarro, J. F., Abadi, M. G., & Steinmetz, M. 2005, MNRAS, 359, 93

Mihalas, D., & Binney, J. 1981, Galactic Astronomy (2nd ed.; San Francisco: W.H. Freeman)

Morrison, H.L., Flynn, C., & Freeman, K.C. 1990, AJ, 100, 1191

Morrison, H.L., et al. 2003, AJ, 125, 2502

Navarro, J. F., Helmi, A., & Freeman, K. C. 2004, ApJ, 601, L43

Nissen, P. E., & Schuster, W. J. 1997, A&A, 326, 751

Nordström, B., et al. 2004, A&A, 418, 989

Norris, J., Bessell, M. S., & Pickles, A. J. 1985, ApJS, 58, 463

Pilachowski, C. A., Sneden, C., & Kraft, R. P. 1996, AJ, 111, 1689

Royston, P. 1995, Applied Statistics, 44, 547

Schuster, W. J., Beers, T. C., Michel, R., Nissen, P. E., & García, G. 2004, A&A, 422, 527

Schwarzschild, K. 1907, Nachrichten von der Königlichen Gesellschaft der Wissenschaften zu Göttingen, –, 614

Searle, L. & Zinn, R. 1978, ApJ, 225, 357

Shapiro, S.S. & Wilk, M.B. 1965, Biometrika, 52, 591

Shetrone, M. D., Côté, P., & Sargent, W. L. W. 2001, ApJ, 548, 592

Shetrone, M., Venn, K. A., Tolstoy, E., Primas, F., Hill, V., & Kaufer, A. 2003, AJ, 125, 684

Steinmetz, M. & Muller, E. 1994, A&A, 281, L97.

Steinmetz, M., et al. 2006, AJ, 132, 1645

Stephens, A., & Boesgaard, A. M. 2002, AJ, 123, 1647

Stephens, M. A. 1986, in Goodness-of-Fit Technqiues. ed. R. B. D'Agostino & M. A. Stephens (New York: Dekker), 195

Tolstoy, E., Venn, K. A., Shetrone, M., Primas, F., Hill, V., Kaufer, A., & Szeifert, T. 2003, AJ, 125, 707

Turon, C., O'Flaherty, K. S., & Perryman, M. A. C. 2005, ESA SP-576: The Three-Dimensional Universe with Gaia

Twarog, B. A. & Anthony-Twarog, B. J. 1994, AJ, 107, 1371

Urban, S. E., Corbin, T. E., & Wycoff, G. L. 1998, AJ, 115, 2161

Vedel, H., & Sommer-Larsen, J. 1990, ApJ, 359, 104

Venn, K. A., Irwin, M., Shetrone, M. D., Tout, C. A., Hill, V., & Tolstoy, E. 2004, AJ, 128, 1177

Vivas, A. K., & Zinn, R. 2006, AJ, 132, 714

Vivas, A. K., Zinn, R., & Gallart, C. 2005, AJ, 129, 189

Willman, B., Dalcanton, J., Ivezić, Ž., Jackson, T., Lupton, R., Brinkmann, J., Hennessy, G., & Hindsley, R. 2002, AJ, 123, 848

White, S. D. M. & Springel, V. 2000, in The First Stars, ed. A. Weiss, T. G. Abel, V. Hill (Berlin: Springer–Verlag), 327

Zinn, R. 1985, ApJ, 293, 424

This preprint was prepared with the AAS LaTeX macros v5.2.

Table 1. Combined Sample Red Giants and RHB stars (see Section 2.2 for details and M07 for the RR Lyrae data).

Name	RV km s^{-1}	D kpc	δ D kpc	[Fe/H]	v_r km s^{-1}	δ v_r km s^{-1}	v_ϕ km s^{-1}	δ v_ϕ km s^{-1}	v_z km s^{-1}	δ v_z km s^{-1}	Source
HD 20	-57.4	0.46	0.07	-1.66	204.40	14.5	17.21	14.5	10.89	3.7	CY98
HD 97	76.3	0.47	0.27	-1.38	-259.69	64.2	-67.02	87.0	-124.62	12.2	CY98
CD -23 72	20.2	0.55	0.07	-1.12	-7.90	2.5	163.70	5.4	-24.95	1.3	CY98
HD 2665	-378.5	0.24	0.23	-1.87	-170.94	7.2	-115.51	6.4	-30.19	17.6	CY98
HD 2796	-60.5	0.72	0.10	-2.35	-109.48	10.3	75.47	14.8	34.06	3.3	CY98
HD 3008	-80.8	1.54	0.06	-1.87	53.52	9.0	101.19	8.8	59.41	2.3	CY98
HD 4306	-67.0	0.56	0.09	-2.72	148.75	16.3	168.14	4.7	84.93	1.7	CY98
BD -11 145	-93.4	1.85	0.17	-2.02	-134.52	24.7	31.84	31.7	24.58	11.3	CY98
HD 5426	27.7	0.72	0.13	-2.33	-42.74	5.2	26.02	26.2	2.42	3.2	CY98
BD -20 170	-5.3	0.76	0.24	-1.31	57.98	16.4	163.41	16.7	11.70	1.1	CY98
CD -30 298	29.7	1.00	0.06	-3.09	317.63	19.4	150.99	6.3	-18.08	1.1	CY98
HD 6446	62.0	0.62	···	-1.60	-7.44	···	65.70	···	90.00	···	B00
HD 6755	-328.7	0.17	0.18	-1.62	207.21	72.1	-326.56	50.3	110.96	16.7	CY98
HD 8724	-110.2	0.73	0.08	-1.76	-15.71	4.7	-98.77	22.6	-74.52	13.1	CY98
HD 9051	-72.7	0.45	0.24	-1.50	46.04	15.9	138.74	22.8	92.25	3.5	CY98
BD -18 271	-209.3	2.38	0.05	-2.06	-164.37	13.6	-56.22	19.6	167.03	3.8	CY98
HD 13979	54.0	0.80	0.09	-2.63	-37.37	4.9	13.89	20.5	-17.58	3.0	CY98
BD -22 395	103.1	1.69	0.14	-2.14	68.62	7.8	-158.56	54.3	-25.28	9.7	CY98
BD -10 548	238.7	0.83	0.18	-1.71	280.40	32.3	-16.24	46.9	-77.54	23.4	CY98
CD -36 1052	306.0	0.72	0.07	-2.19	87.54	3.9	137.36	3.7	-267.16	4.8	CY98
CD -30 1121	103.9	0.78	0.20	-1.82	12.83	2.9	51.98	28.0	-35.05	10.9	CY98
HD 21022	110.0	1.19	0.11	-1.99	-25.13	7.7	-44.88	24.2	8.85	10.3	CY98
HD 21581	154.2	0.39	0.15	-1.74	94.47	2.0	38.03	27.8	-97.11	1.5	CY98
CD -24 1782	118.5	0.73	0.08	-2.37	-137.14	16.8	-276.76	38.1	8.50	9.0	CY98
HD 23798	89.5	1.06	0.09	-1.90	54.58	4.6	126.96	6.8	-5.61	5.8	CY98
HD 25532	-112.5	0.27	0.11	-1.23	-88.13	2.9	25.51	21.0	25.75	2.5	CY98
HD 26297	13.5	0.62	0.08	-1.76	31.91	3.3	134.86	8.1	80.72	7.1	CY98
BD +06 648	-141.4	1.25	0.06	-2.04	-163.11	3.6	-44.47	17.0	72.42	4.8	CY98
HD 27928	15.1	0.64	0.16	-2.25	-161.56	24.1	65.80	23.1	43.86	8.0	CY98
HD 29574	23.8	1.17	···	-1.55	-213.25	···	54.53	···	-168.71	···	CY98
HD 30229	304.1	0.61	0.13	-2.32	-122.47	12.5	-74.23	8.0	-92.45	11.8	CY98
HD 32546	157.0	0.53	0.18	-1.30	41.00	26.0	94.33	11.9	-57.00	9.4	B00
HD 268957	172.3	0.57	0.07	-1.63	316.13	26.2	50.47	4.9	-102.88	2.7	CY98
HD 36702	121.8	1.12	0.09	-1.86	-51.10	9.0	90.09	4.8	-53.21	2.8	CY98
HD 274939	190.0	0.47	0.23	-1.67	-221.86	56.7	-9.70	18.5	-103.69	7.1	CY98
HD 37828	185.0	0.31	···	-1.43	77.58	···	70.59	···	-32.00	···	B00
HD 41667	302.0	0.53	0.19	-1.18	272.66	27.6	72.90	12.5	-32.00	14.2	B00
HD 44007	165.3	0.15	0.18	-1.61	83.42	5.5	81.16	8.5	9.53	7.5	CY98
HD 74462	-168.1	0.79	0.12	-1.53	-121.39	1.9	-165.61	40.9	142.10	29.2	CY98
HD 82590	215.6	0.53	0.07	-1.85	-186.61	17.8	-120.53	11.0	-34.38	9.7	CY98
HD 83212	109.5	0.68	0.11	-1.49	10.99	2.1	102.12	3.9	-24.21	8.6	CY98
HD 233666	-65.5	0.53	0.07	-1.65	-70.53	2.2	151.65	5.1	-2.56	3.0	CY98
HD 84903	79.0	0.86	0.04	-2.55	24.29	3.3	147.25	5.1	-42.67	3.9	CY98
HD 237846	-302.8	0.82	0.10	-2.67	-199.16	3.1	116.48	4.7	-195.83	3.1	CY98
HD 85773	148.8	1.82	0.05	-2.18	28.81	7.5	2.31	6.3	-150.74	13.1	CY98

Table 1—Continued

Name	RV km s^{-1}	D kpc	δ D kpc	[Fe/H]	v_r km s^{-1}	δ v_r km s^{-1}	v_ϕ km s^{-1}	δ v_ϕ km s^{-1}	v_z km s^{-1}	δ v_z km s^{-1}	Source
HD 88609	-36.2	1.01	0.05	-2.69	-38.55	3.5	81.27	8.8	27.57	3.7	CY98
BD +30 2034	97.0	2.48	···	-1.52	211.71	···	53.94	···	-42.00	···	B00
CD -30 8626	262.0	0.73	0.24	-1.67	-48.20	10.1	-69.76	14.0	-12.91	31.8	CY98
HD 93529	143.0	0.41	0.26	-1.24	-28.59	4.6	57.89	12.6	-7.21	22.2	CY98
BD +04 2466	37.6	0.38	0.16	-1.85	-28.08	3.9	109.01	16.5	-18.67	9.2	CY98
HD 99978	68.0	0.31	···	-1.12	-74.79	···	185.40	···	-12.00	···	B00
CPD -70 1436	300.0	0.51	···	-2.10	107.58	···	-149.74	···	-65.51	···	CY98
BD +22 2411	34.5	2.23	0.08	-1.95	-15.58	13.1	51.47	17.6	7.74	4.6	CY98
TY Vir	229.0	0.72	0.07	-1.58	7.05	3.3	-62.91	12.4	82.06	8.9	CY98
BD -01 2582	0.2	0.36	0.10	-2.32	-76.80	6.7	63.52	16.3	-95.28	10.6	CY98
HD 103545	179.7	1.05	0.09	-2.42	126.10	12.1	-89.00	23.6	62.02	10.1	CY98
HD 104053	-56.0	1.07	···	-1.10	43.12	···	95.87	···	-76.00	···	B00
BD +09 2574	-48.8	1.12	0.18	-1.95	-82.81	15.4	23.08	42.6	-125.17	16.6	CY98
HD 104893	23.6	1.40	0.06	-1.86	141.05	11.3	112.42	7.7	-60.81	6.1	CY98
HD 105546	19.3	0.36	0.07	-1.44	9.38	1.0	118.81	8.8	75.91	4.1	CY98
HD 106373	96.0	0.43	0.07	-2.48	163.41	14.9	84.69	10.8	67.59	6.6	CY98
HD 107752	220.0	1.36	0.09	-2.68	142.30	15.2	-175.08	31.1	118.59	8.8	CY98
HD 108317	6.5	0.32	0.08	-2.34	188.70	16.1	76.32	12.6	-25.42	3.3	CY98
[MFF90] PHI 2/2 97	12.0	2.42	···	-1.10	50.85	···	134.13	···	-73.00	···	B00
HD 108577	-111.7	1.04	0.09	-2.50	209.15	18.1	-105.27	31.1	-191.99	7.6	CY98
BD +04 2621	-42.0	1.46	0.08	-2.34	-1.75	9.4	-8.70	21.7	-138.08	8.9	CY98
BD +30 2294	56.0	1.81	···	-1.09	-4.91	···	47.01	···	71.00	···	B00
BD +26 2368	100.0	1.26	···	-1.08	-76.95	···	115.37	···	110.00	···	B00
HD 109823	8.0	0.83	···	-1.68	-11.10	···	150.99	···	21.00	···	B00
HD 110184	140.1	1.22	0.04	-2.31	12.84	5.2	104.94	5.0	119.10	1.6	CY98
HD 110281	141.6	2.48	···	-1.75	-276.64	···	-101.01	···	-34.03	···	CY98
CD -27 8864	247.0	1.77	···	-1.71	82.62	···	-126.86	···	37.00	···	B00
BD +33 2273	41.0	1.46	···	-1.05	66.17	···	81.06	···	63.00	···	B00
HD 112126	-62.0	1.30	···	-1.52	41.24	···	17.45	···	-32.00	···	B00
BD +10 2495	252.9	0.78	0.17	-2.14	136.83	35.0	175.60	4.0	288.68	7.3	CY98
BD +12 2547	5.7	1.47	0.11	-2.07	-233.94	24.4	-66.87	29.9	-91.91	10.9	CY98
HD 115444	-27.6	0.78	0.08	-2.63	-156.34	12.2	63.50	13.6	13.33	5.7	CY98
BD +03 2782	32.0	1.82	···	-2.02	146.92	···	38.17	···	57.00	···	B00
HD 118055	-101.0	1.13	0.06	-1.76	100.29	5.6	161.94	8.3	-98.11	3.3	CY98
BD +18 2757	-22.2	1.34	0.09	-2.52	-28.41	5.5	29.14	21.5	-25.34	1.8	CY98
HD 119516	-287.0	0.51	0.07	-2.49	145.36	5.4	143.15	7.5	-250.47	1.6	CY98
HD 121135	126.4	0.87	0.19	-1.83	-2.38	13.2	62.53	28.9	118.71	1.7	CY98
HD 121261	99.4	1.30	0.14	-1.52	78.77	19.7	5.80	21.9	42.21	4.2	CY98
HD 122563	-24.8	0.31	0.06	-2.55	142.80	8.3	-20.03	14.8	27.63	2.7	CY98
HD 122956	166.3	0.36	0.11	-1.74	-21.75	9.4	19.50	16.4	122.18	1.2	CY98
HD 124358	325.0	1.13	0.12	-1.98	104.03	38.7	-290.72	55.5	313.68	8.8	CY98
BD +09 2860	-19.0	1.04	0.07	-1.67	-161.42	13.1	105.27	12.5	-97.97	7.1	CY98
BD +09 2870	-120.7	1.35	0.06	-2.39	306.41	16.8	22.15	15.2	22.55	8.0	CY98
BD +01 2916	-12.7	1.92	0.07	-1.61	81.75	8.7	3.16	18.1	13.73	4.7	CY98
BD +08 2856	64.5	2.45	0.07	-2.02	-261.61	19.7	116.59	15.6	-62.71	11.2	CY98

Table 1—Continued

Name	RV km s^{-1}	D kpc	δ D kpc	[Fe/H]	v_r km s^{-1}	δ v_r km s^{-1}	v_ϕ km s^{-1}	δ v_ϕ km s^{-1}	v_z km s^{-1}	δ v_z km s^{-1}	Source
HD 126238	247.0	0.24	0.14	-1.85	-209.36	4.3	42.51	5.6	-39.14	16.8	CY98
HD 126587	149.2	0.62	0.08	-2.79	-121.34	2.2	37.26	10.8	-3.52	8.2	CY98
HD 128279	-81.7	0.16	0.22	-2.22	-21.13	15.4	140.32	27.3	-252.33	49.9	CY98
BD +30 2611	-278.2	1.11	0.10	-1.26	13.91	9.0	155.60	4.6	-276.18	4.7	CY98
BD +18 2976	-173.1	1.69	0.07	-2.42	24.24	10.7	-155.61	26.5	-77.57	7.6	CY98
HD 135148	-91.9	1.11	0.05	-1.88	135.17	6.5	127.27	6.8	13.10	5.2	CY98
HD 135449	-23.0	0.45	0.07	-1.47	155.07	14.4	-0.11	18.3	76.97	7.5	CY98
HD 136316	-45.0	0.50	0.08	-2.00	96.81	11.9	147.78	11.4	-87.96	7.5	CY98
BD +01 3070	-329.4	0.50	0.23	-1.85	343.77	27.3	273.99	12.6	-112.58	26.0	CY98
HD 141531	2.6	1.29	0.13	-1.57	-182.48	23.1	-66.32	36.9	-52.25	10.7	CY98
BD +05 3098	-160.5	1.23	0.12	-2.40	28.43	11.1	-205.59	47.2	-65.18	10.9	CY98
BD +11 2998	50.2	0.42	0.07	-1.22	-54.74	1.5	36.03	15.3	155.52	8.6	CY98
BD +09 3223	67.0	0.50	0.07	-2.41	-191.27	9.6	32.33	16.3	9.54	3.4	CY98
BD +17 3248	-145.6	0.51	0.21	-2.07	59.78	7.4	50.73	20.2	16.20	15.3	CY98
CD -68 1881	134.0	1.19	0.33	-1.81	-62.26	28.0	153.98	19.6	-173.00	50.7	B00
HD 165195	-0.2	0.65	0.03	-2.42	-151.91	6.1	14.94	7.2	-30.55	2.3	CY98
HD 166161	68.4	0.20	0.15	-1.27	-146.25	9.9	72.32	26.6	9.01	1.2	CY98
HD 175305	-181.0	0.12	0.19	-1.54	32.51	17.0	128.72	10.7	-222.72	30.1	CY98
HD 174578	-4.0	1.10	0.36	-1.69	-1.42	10.0	350.17	37.9	94.00	28.3	B00
HD 184266	-348.4	0.22	0.07	-1.87	298.37	1.0	-50.17	10.4	-98.31	14.5	CY98
HD 184711	101.6	1.01	0.04	-2.30	-74.43	2.4	-0.15	9.3	-104.23	4.4	CY98
HD 232078	-391.0	0.83	···	-1.61	137.49	···	-136.65	···	-75.00	···	B00
HD 186478	30.9	1.02	0.06	-2.45	-192.92	9.2	-137.86	25.3	-67.16	6.0	CY98
HD 187111	-181.0	0.61	0.18	-1.95	137.06	2.9	24.79	21.5	-99.15	28.6	CY98
BD -18 5550	-126.2	0.74	0.08	-2.84	36.96	5.1	-98.39	22.6	-96.32	12.6	CY98
HD 190287	135.0	0.14	0.23	-1.09	-136.43	3.5	129.59	26.3	-63.15	1.9	CY98
HD 195636	-257.8	0.59	0.07	-2.82	-36.60	14.4	-141.82	17.0	166.43	4.5	CY98
BD -17 6036	19.2	1.27	0.09	-2.70	-200.00	17.0	17.60	22.3	52.15	11.6	CY98
BD -15 5781	-76.4	1.93	0.08	-2.47	16.04	7.5	26.02	18.7	-61.81	12.6	CY98
BD -14 5890	117.5	0.93	0.19	-2.01	-267.26	30.9	-19.80	60.3	-130.64	13.5	CY98
CD -37 14010	-200.0	1.68	···	-2.55	244.98	···	-94.42	···	-33.00	···	B00
HD 200654	-48.0	0.46	0.06	-2.79	382.45	21.2	-344.74	34.4	-225.92	15.9	CY98
BD -03 5215	-293.7	0.73	0.07	-1.72	147.76	4.3	-30.82	5.8	96.55	7.1	CY98
HD 204543	-98.2	0.72	0.11	-1.69	-32.91	9.8	47.15	14.9	-5.24	7.5	CY98
HD 205547	47.0	1.10	···	-1.85	-190.90	···	46.41	···	103.00	···	B00
HD 206739	-57.8	0.57	···	-1.58	78.66	···	115.51	···	-54.51	···	CY98
BD -09 5831	14.5	1.90	0.13	-1.87	-68.55	13.2	126.24	17.0	-56.01	9.2	CY98
HD 235766	-314.0	0.92	···	-2.35	-315.17	···	6.82	···	3.00	···	B00
HD 214362	-92.3	0.49	0.07	-2.20	321.17	21.0	-20.30	15.4	-133.39	15.4	CY98
HD 214925	-328.0	2.15	0.08	-2.14	93.56	9.5	-289.91	36.1	143.00	14.0	B00
HD 216143	-115.9	0.69	0.07	-2.20	-327.79	25.1	-29.90	15.9	76.35	2.4	CY98
HD 218857	-169.6	0.41	0.19	-2.15	-129.95	32.0	44.21	23.7	153.77	1.2	CY98
HD 220662	-78.1	1.87	0.08	-1.59	0.33	11.2	10.05	17.2	37.78	5.0	CY98
HD 220838	-22.8	1.43	0.07	-1.72	-24.64	8.4	149.05	8.0	22.65	3.1	CY98
HD 221170	-121.9	0.69	0.07	-2.01	-151.22	8.6	93.53	3.3	-62.75	8.8	CY98

Table 1—Continued

Name	RV km s^{-1}	D kpc	δ D kpc	[Fe/H]	v_r km s^{-1}	δ v_r km s^{-1}	v_ϕ km s^{-1}	δ v_ϕ km s^{-1}	v_z km s^{-1}	δ v_z km s^{-1}	Source
HD 222434	13.4	0.97	0.14	-1.56	-98.84	12.2	43.08	26.1	10.87	3.6	CY98

Table 2. Smooth Halo Model Parameters

	With H99 Streams	Without H99 Streams
$\langle v_R \rangle$	-0.93 ± 10.20	-3.57 ± 10.63
σ_R	154.96 ± 7.21	157.30 ± 7.52
$\langle v_\phi \rangle$	28.62 ± 7.19	23.42 ± 7.41
σ_ϕ	109.33 ± 5.09	109.64 ± 5.24
$\langle v_z \rangle$	-6.43 ± 6.66	-1.32 ± 5.66
σ_z	101.23 ± 4.71	83.75 ± 4.00

Table 3. Shapiro-Wilk Results for H99 data

Data Set	N_{stars}	p-value
All Stars	101	0.009
Excluding H99 Streams	94	0.05
Excluding H99 Streams & HD 124358	93	0.19

Table 4. H99 Stream Stars in Combined Data Set

Name	RV km s^{-1}	D kpc	δ D kpc	[Fe/H]	v_r km s^{-1}	δv_r km s^{-1}	v_ϕ km s^{-1}	δv_ϕ km s^{-1}	v_z km s^{-1}	δv_z km s^{-1}	Source
CD -36 1052	306.0	0.72	0.07	-2.19	87.54	3.9	137.36	3.7	-267.16	4.8	CY98
AS CNC	258.0	2.31	0.16	-1.89	16.09	39.7	38.16	54.2	363.00	49.4	M06
TT CNC	47.0	1.22	0.09	-1.58	106.04	12.0	87.25	13.8	-231.10	22.0	M06
TT LYN	-67.0	0.65	0.05	-1.76	124.42	13.0	106.61	8.8	-233.30	13.9	M06
HD 237846	-302.8	0.82	0.10	-2.67	-199.16	3.1	116.48	4.7	-195.83	3.1	CY98
BD +10 2495	252.9	0.78	0.17	-2.14	136.83	35.0	175.60	4.0	288.68	7.3	CY98
HD 119516	-287.0	0.51	0.07	-2.49	145.36	5.4	143.15	7.5	-250.47	1.6	CY98
HD 128279	-81.7	0.16	0.22	-2.22	-21.13	15.4	140.32	27.3	-252.33	49.9	CY98
BD +30 2611	-278.2	1.11	0.10	-1.26	13.91	9.0	155.60	4.6	-276.18	4.7	CY98
AR SER	127.0	1.71	0.12	-1.78	98.02	21.3	100.60	24.8	313.40	23.1	M06
HD 175305	-181.0	0.12	0.19	-1.54	32.51	17.0	128.72	10.7	-222.72	30.1	CY98
XZ CYG	-146.0	0.50	0.04	-1.52	26.64	4.5	152.18	11.9	-232.50	15.2	M06

Table 5. Retrograde Outlier Stars in Combined Data Set

Name	RV km s^{-1}	D kpc	δ D kpc	[Fe/H]	v_r km s^{-1}	δv_r km s^{-1}	v_ϕ km s^{-1}	δv_ϕ km s^{-1}	v_z km s^{-1}	δv_z km s^{-1}	Source
HD 6755	-328.7	0.17	0.18	-1.62	207.21	72.1	-326.56	50.3	110.96	16.7	CY98
CD -24 1782	118.5	0.73	0.08	-2.37	-137.14	16.8	-276.76	38.1	8.50	9.0	CY98
HD 124358	325.0	1.13	0.12	-1.98	104.03	38.7	-290.72	55.5	313.68	8.8	CY98
RV CAP	-84.0	1.06	0.07	-1.72	-69.03	9.5	-279.92	34.3	-193.70	18.3	M06
HD 200654	-48.0	0.46	0.06	-2.79	382.45	21.2	-344.74	34.4	-225.92	15.9	CY98
HD 214925	-328.0	2.15	0.08	-2.14	93.56	9.5	-289.91	36.1	143.00	14.0	B00

Table 6. Prograde Outlier Stars in Combined Data Set

Name	RV km s^{-1}	D kpc	δ D kpc	[Fe/H]	v_r km s^{-1}	δv_r km s^{-1}	v_ϕ km s^{-1}	δv_ϕ km s^{-1}	v_z km s^{-1}	δv_z km s^{-1}	Source
TV LEO	-97.0	1.84	0.13	-1.97	-113.72	30.4	326.94	24.2	-22.90	20.9	M06
BD +01 3070	-329.4	0.50	0.23	-1.85	343.77	27.3	273.99	12.6	-112.58	26.0	CY98
HD 174578	-4.0	1.10	0.36	-1.69	-1.42	10.0	350.17	37.9	94.00	28.3	B00

Table 7. Probability of Finding Halo Stars in Various Regions of the Angular Momentum Diagram

Group	Number of Stars	Lower Left Corner	Upper Right Corner	$P(n \geq n_*)$	$< n >$
H99 Streams	11	$[500, 1400]$	$[1500, 2500]$	0.00024	2.81
Retrograde Outliers	6	$[-3000, 0]$	$[-1750, 2500]$	0.069	2.86
Prograde Outliers	3	$[2000, 30]$	$[3000, 1200]$	0.69	3.55

Table 8. Shapiro-Wilk test results for combined sample v_z data ($D \leq 2.5$ kpc and [Fe/H] ≤ -1.0)

N	Excluded Groups			p-value
	Prograde ▲	Retrograde ▼	H99 streams •	
231	···	···	···	0.002
219	···	···	X	0.584
216	X	···	X	0.584
210	X	X	X	0.877
213	···	X	X	0.850

Table 9. Shapiro-Wilk test results for combined sample v_ϕ data ($D \leq 2.5$ kpc and [Fe/H] ≤ -1.0)

N	Excluded Groups			p-value
	Prograde ▲	Retrograde ▼	H99 streams •	
231	···	···	···	0.00014
228	X	···	···	1.9e-06
222	X	X	···	0.01
225	···	X	···	0.21
219	···	···	X	0.00061
216	X	···	X	1.1e-05
210	X	X	X	0.068
213	···	X	X	0.41

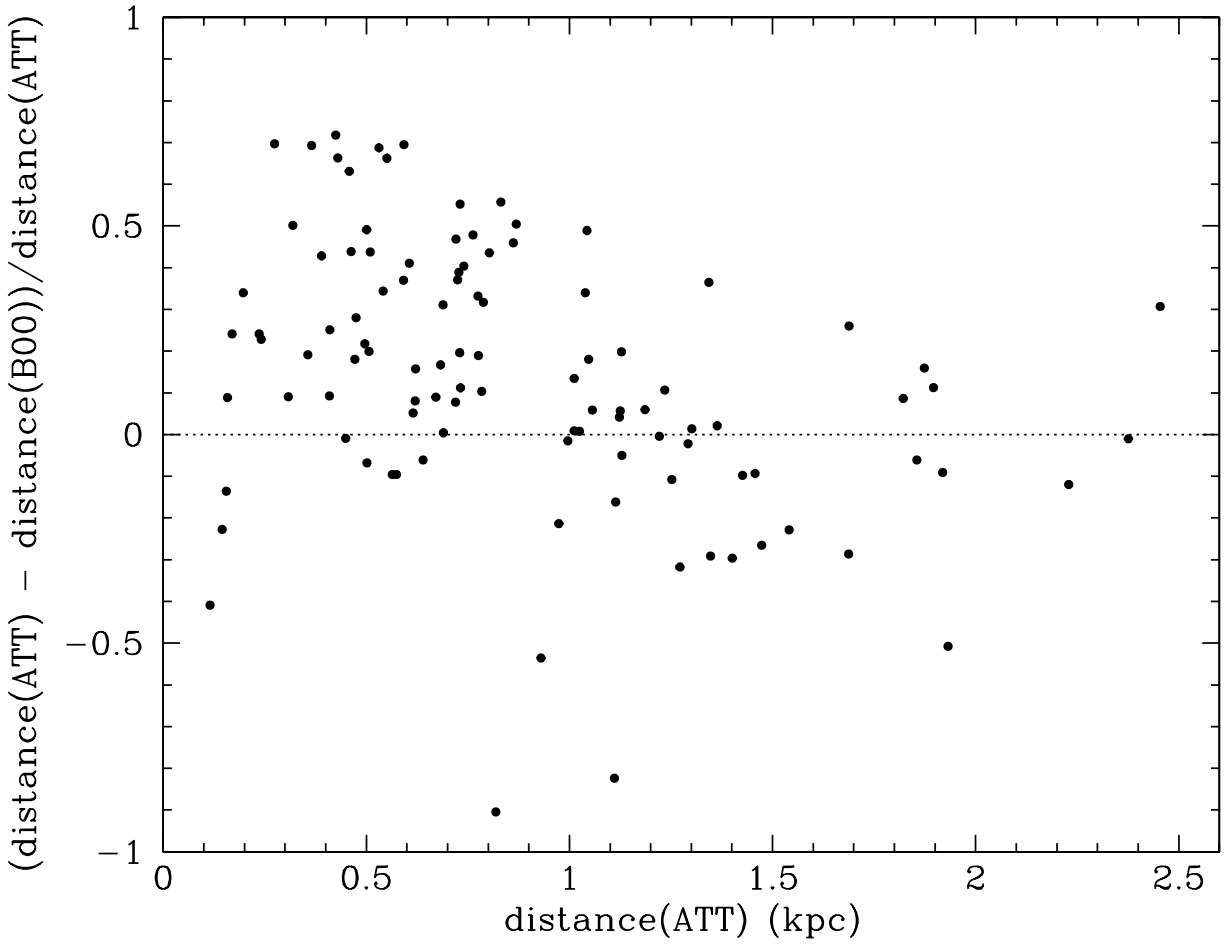


Fig. 1.— Difference between distance estimates for red giants from ATT94 and B00 as a function of distance. The differences are expressed as a fraction of the ATT94 distance. It can be seen that for stars closer than 1 kpc, the B00 distances are on average 40% smaller than the ATT94 distances.

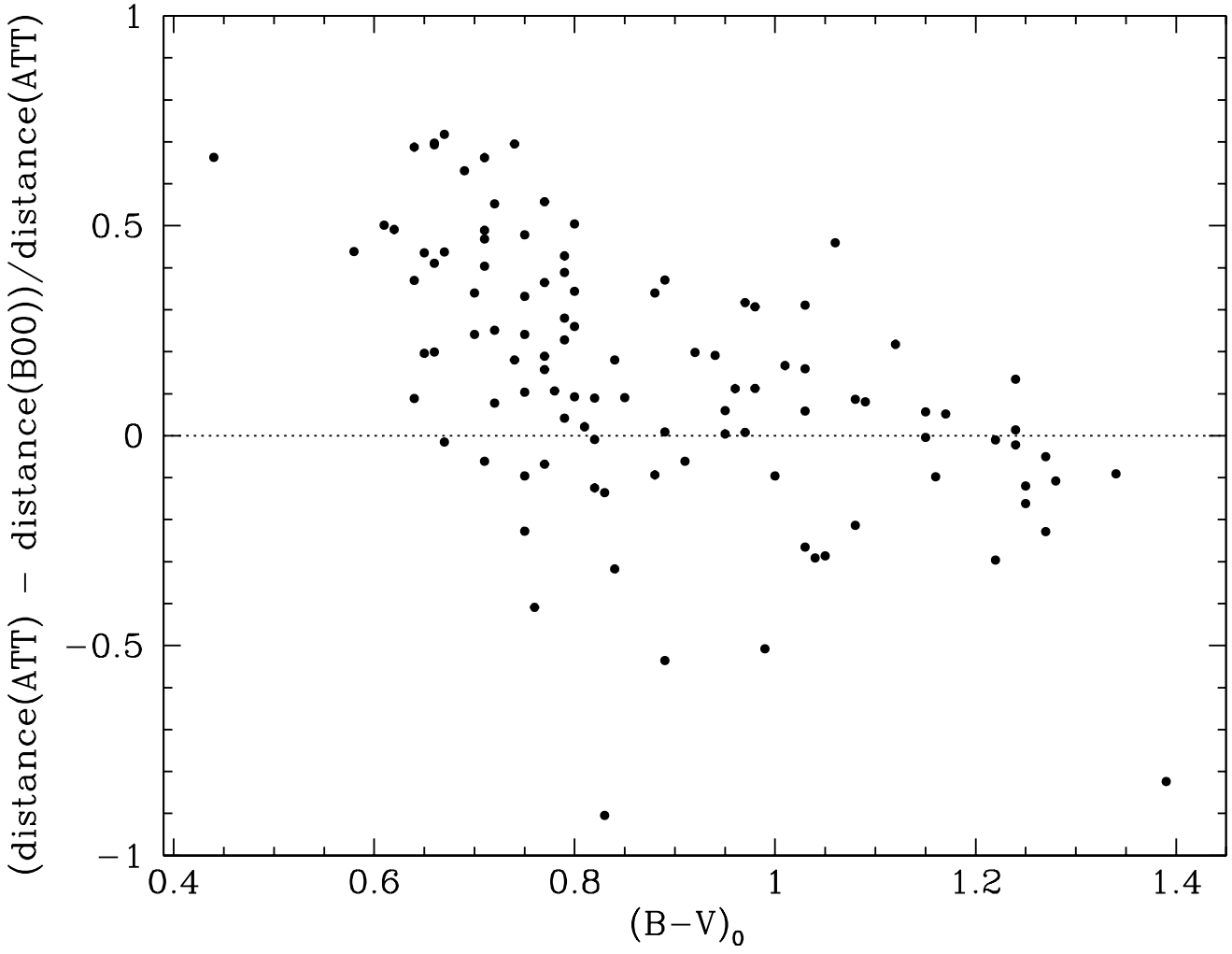


Fig. 2.— Difference between red giant distance estimates from ATT94 and B00, shown as a function of $(B–V)_0$ color. It can now be seen that the problematic stars are the bluest ones, with $(B–V)_0 < 0.9$.

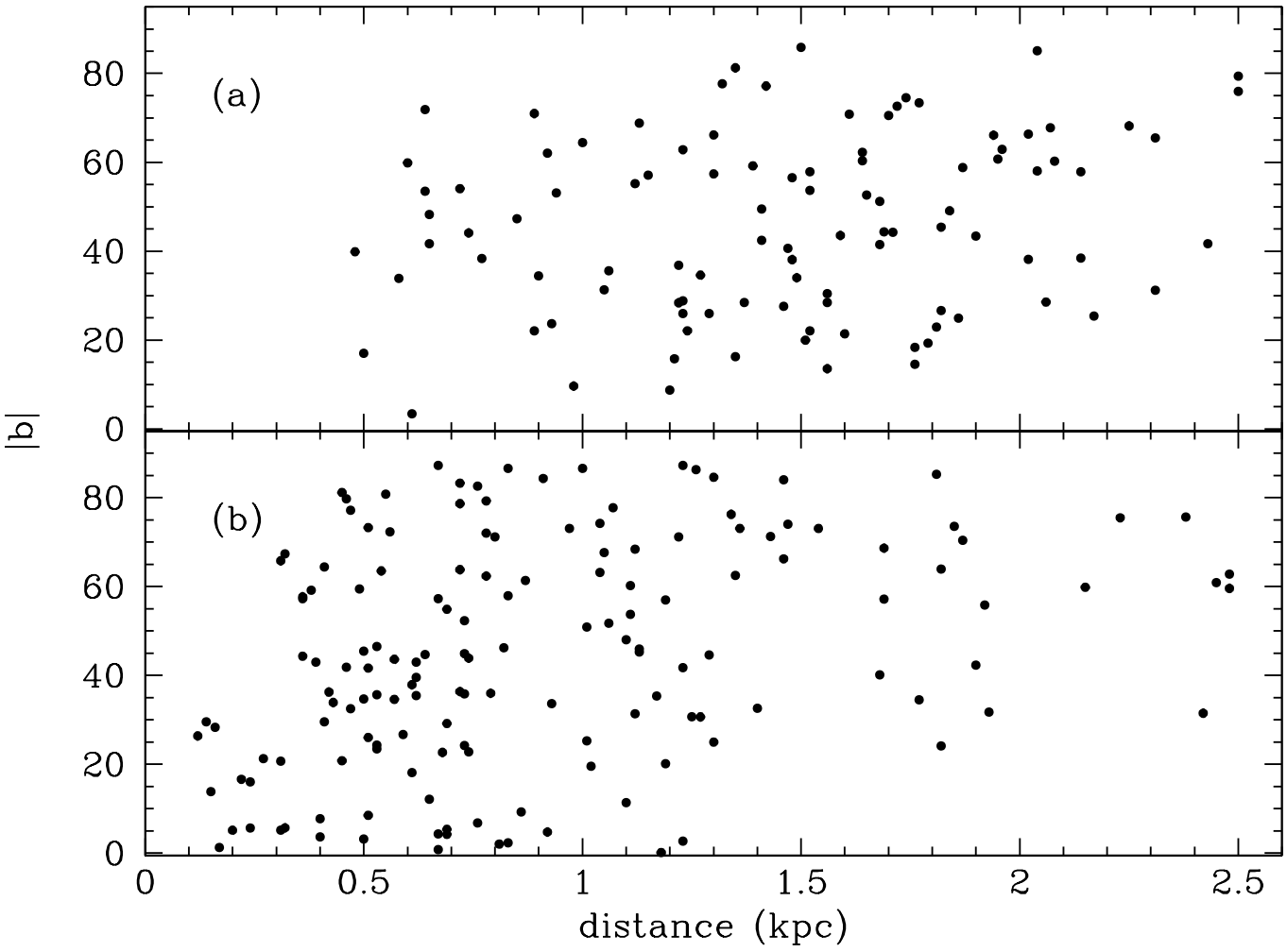


Fig. 3.— Distribution of distance and absolute value of Galactic latitude (b) for (a) the RR Lyrae variables in our sample and (b) the red giant and RHB stars in our sample.

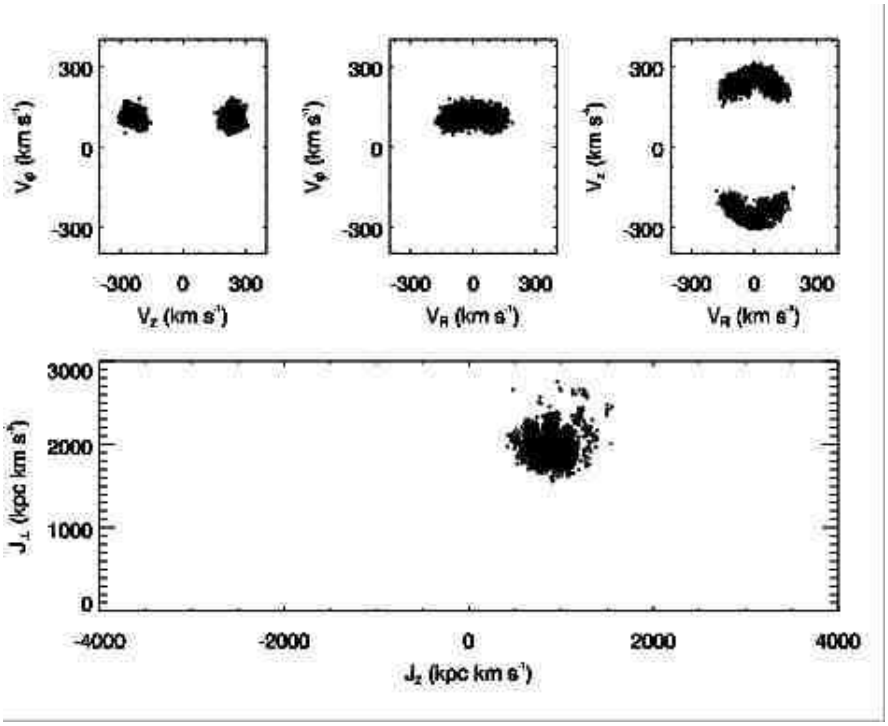


Fig. 4.— Structure in velocity and angular momentum space for the H99 star streams model for stars within 2.5 kpc of the Sun. The bottom panel is a plot of the angular momentum in the plane of the Galaxy's disk as a function of angular momentum out of the disk. The top panels show the cylindrical velocity coordinates of the data plotted against each other.

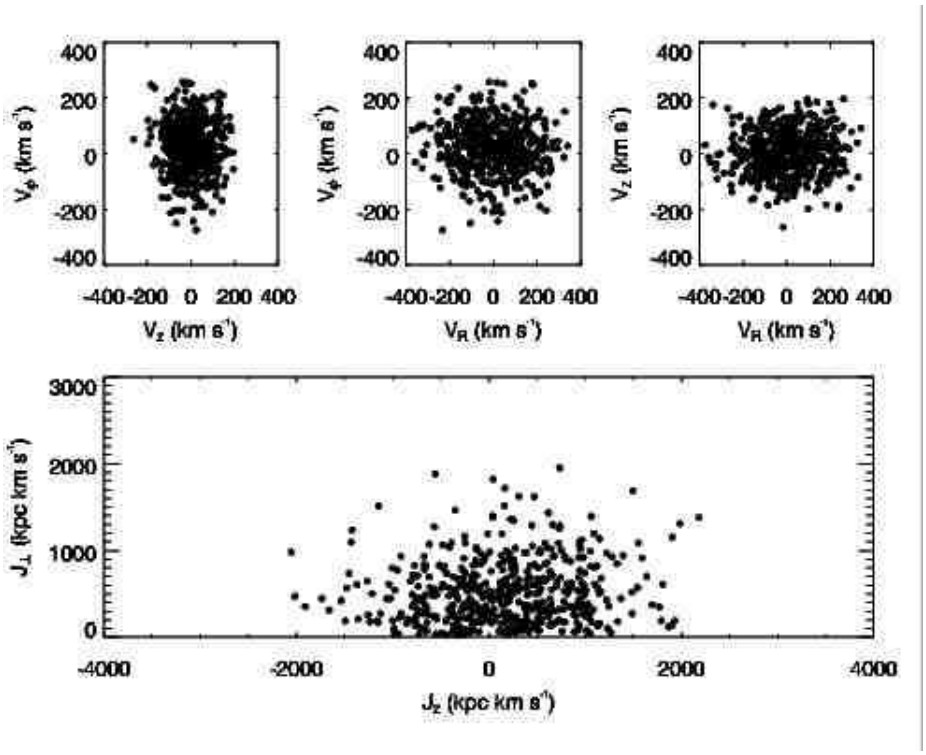


Fig. 5.— Structure in velocity and angular momentum space for the smooth model for stars within 2.5 kpc of the Sun.

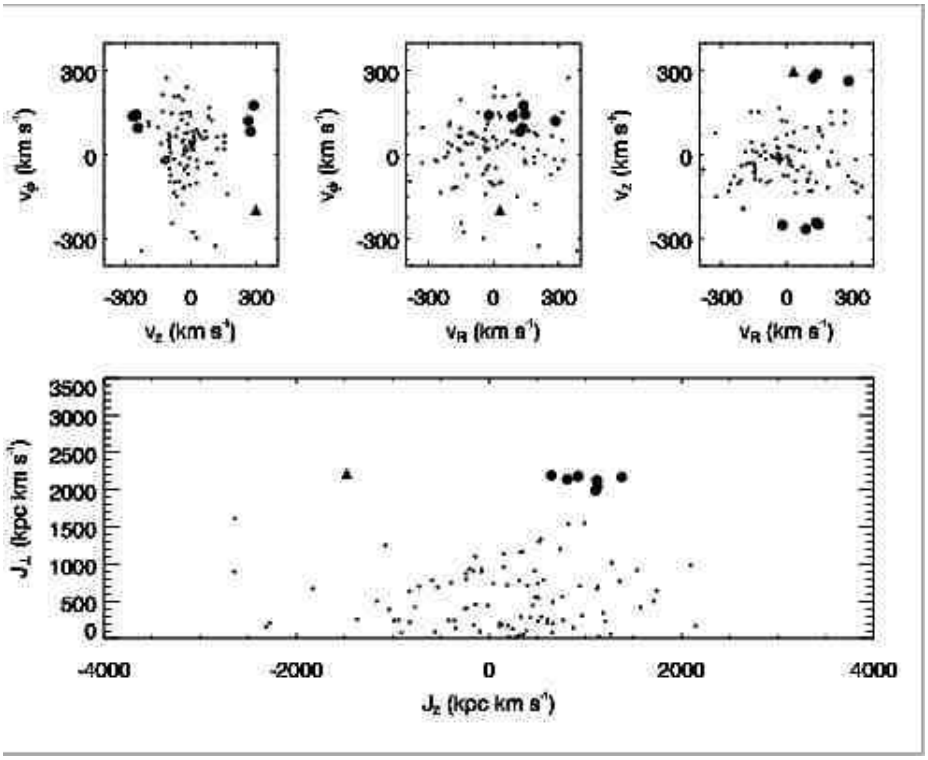


Fig. 6.— Plots of the distribution of the H99 data in velocity and angular momentum space for stars with [Fe/H] ≤ -1.6 and distances less than 1.0 kpc from the Sun. The stream stars are represented by the large circles. The additional v_z outlier (HD 124358) is shown by the upward pointing triangle.

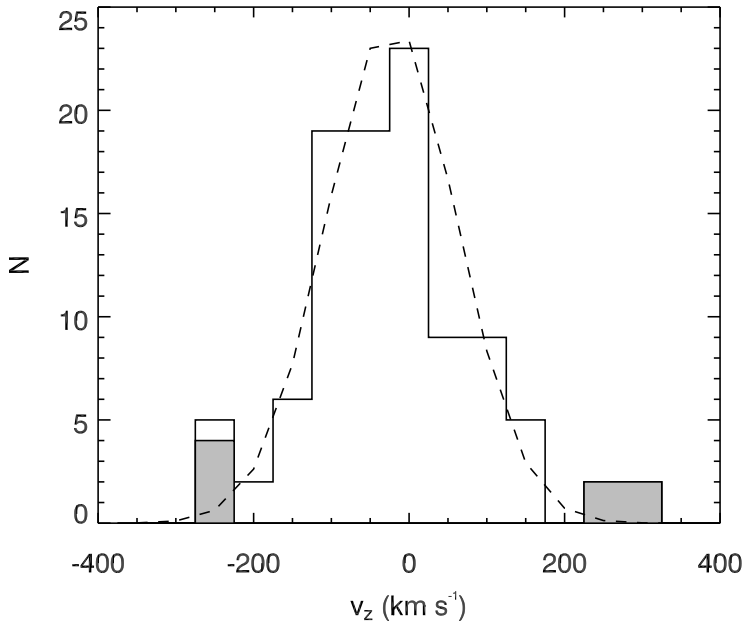


Fig. 7.— Histogram of the H99 data v_z velocity distribution with the stream stars shaded. A normal distribution is plotted as a dashed line. Note how the H99 stream stars widen the wings of the velocity distribution making it deviate from normality.

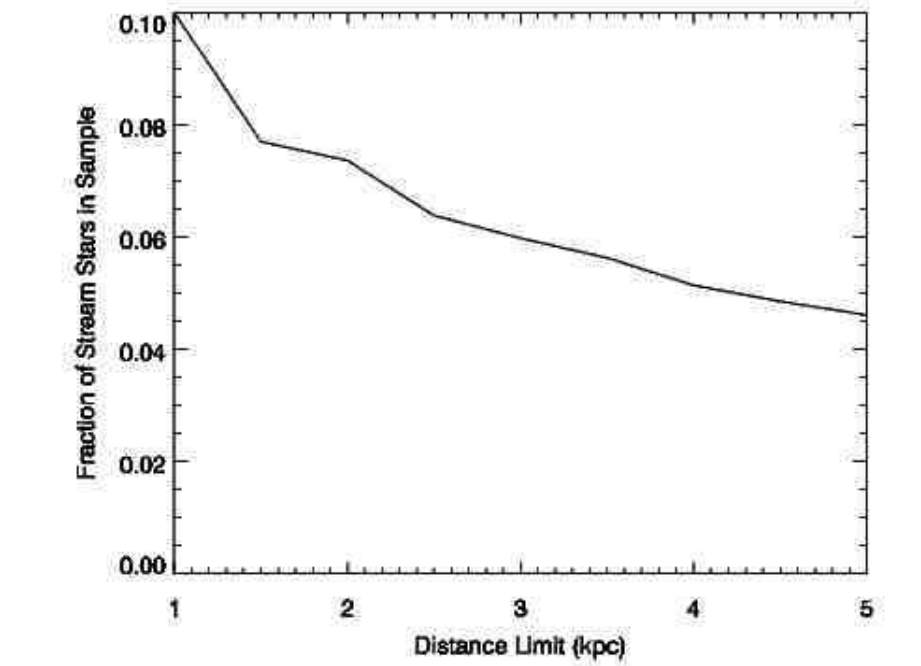


Fig. 8.— Fraction of stream stars in halo as a function of distance limit. Note that the fraction of stream stars decreases as the distance limit increases when the fraction of stream stars is normalized to 10% of the halo stars within 1 kpc of the Sun.

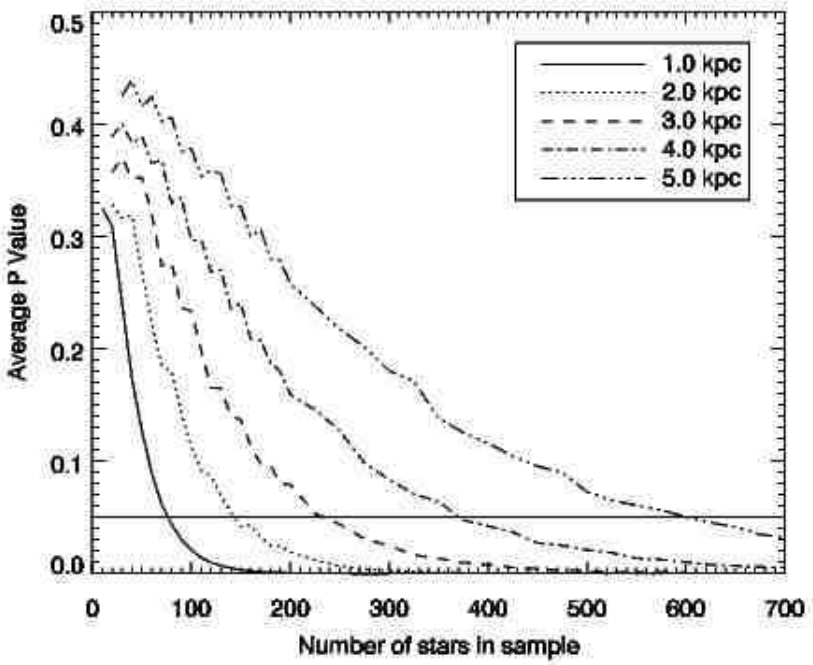


Fig. 9.— Average p-value for 10,000 random samples of v_z velocities with the relative number of stream to smooth halo stars fixed at 10% for a distance limit of 1.0 kpc. The standard deviation of the trial p-values is on the order of the width of the lines. The distance limits used for the samples are 1.0, 2.0, 3.0, 4.0, and 5.0 kpc. As the distance limit increases, the size of the sample for which detections are possible also increases.

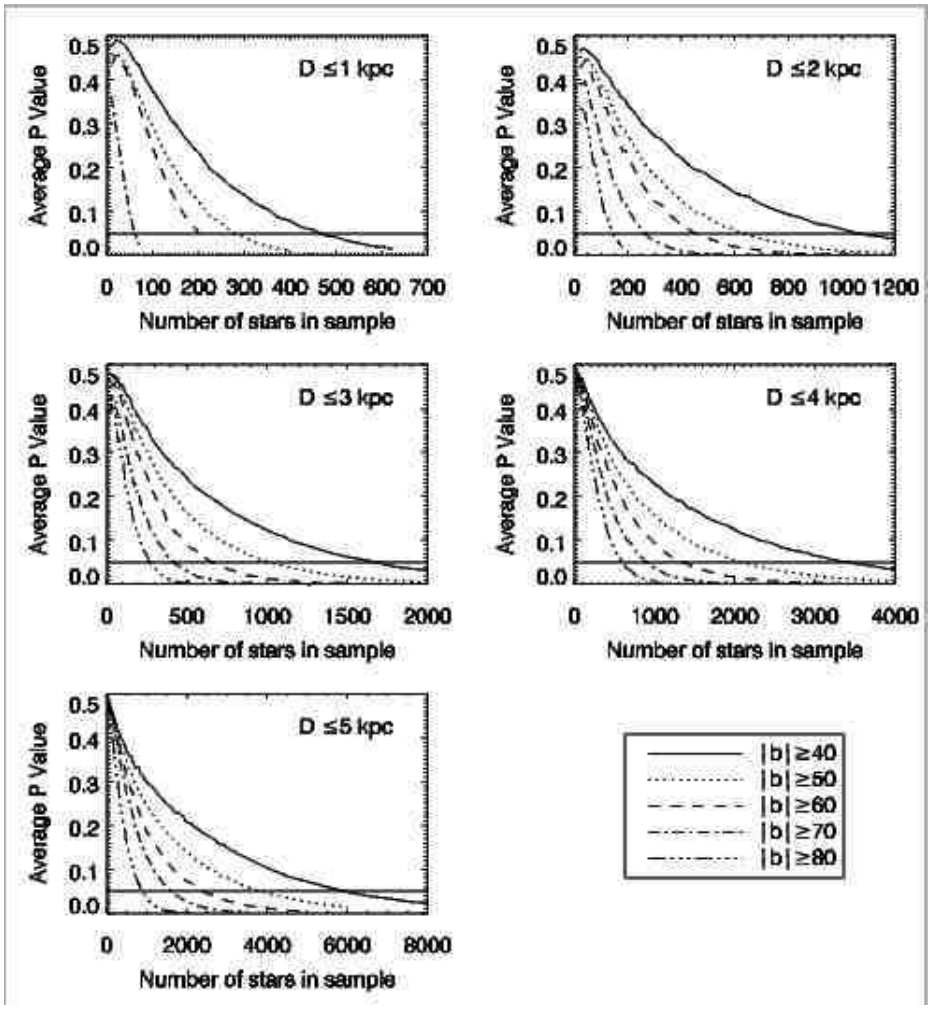


Fig. 10.— Average p-value for 10,000 random samples of radial velocities (corrected to the Galactocentric frame of reference) with 10% stream stars for a distance limit of 1.0 kpc. The standard deviation of the trial p-values is on the order of the width of the lines. Galactic latitude limits ($|b| \geq 40$, $|b| \geq 50$, $|b| \geq 60$, $|b| \geq 70$, and $|b| \geq 80$) were imposed on samples with five different distance limits (1.0, 2.0, 3.0, 4.0, and 5.0 kpc). N.B. The x-axes on these graphs all have different scales, since the range of samples tested is very different in each case.

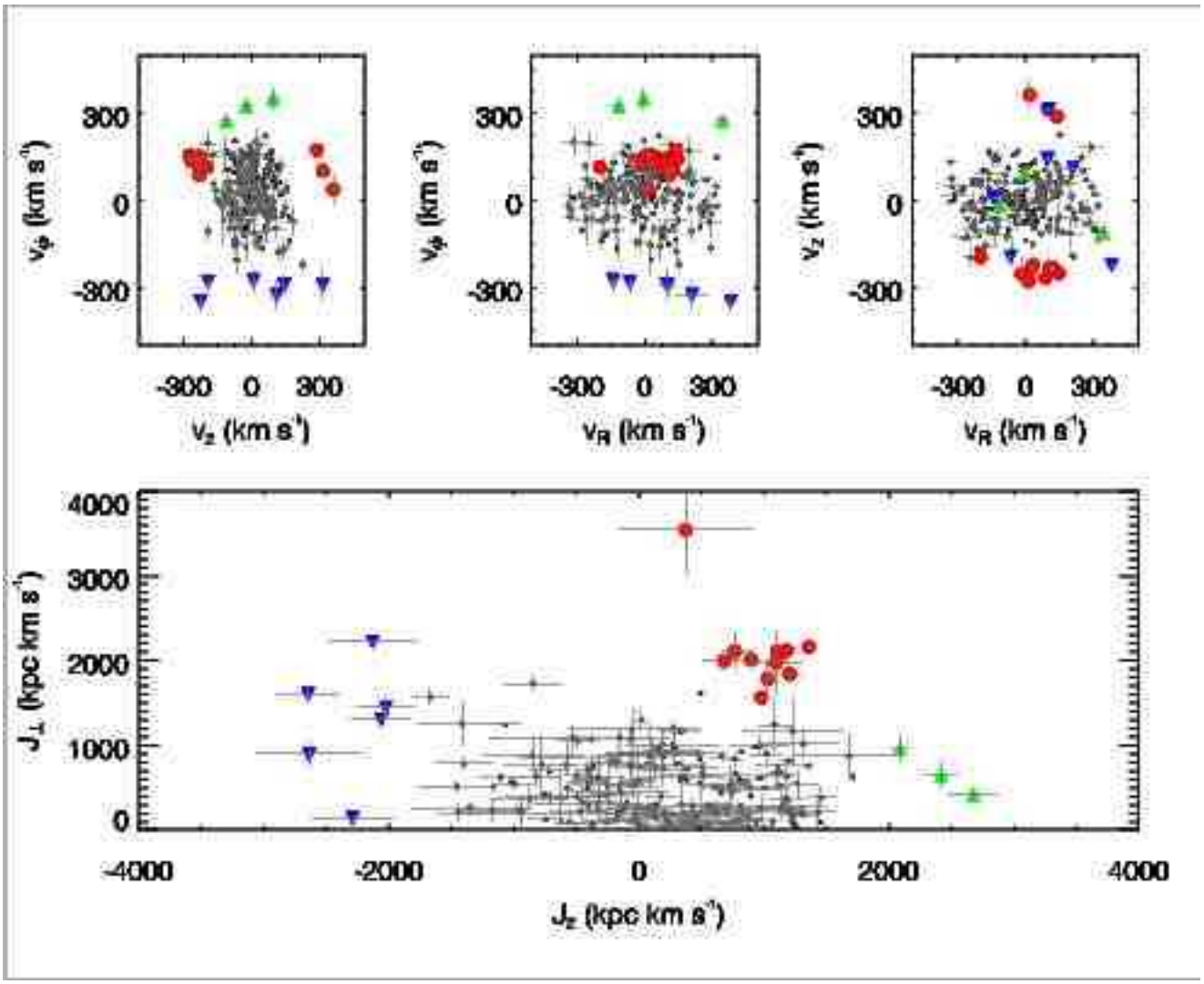


Fig. 11.— Angular momentum and cylindrical velocity plots for the combined data sample with the selection criteria: $D \leq 2.5$ kpc and [Fe/H] ≤ -1.0. The retrograde outliers are indicated by downward0facing triangles, the prograde outliers by upward-facing triangles, and the H99 streams by large circles. Note that the empty region of the angular momentum diagram at $J_z = 1500 - 2500$ kpc km s^{-1}, J$_\perp$ < 600 kpc km s^{-1} was occupied by likely thick-disk stars. These stars were excluded from our final sample based on their position in the angular momentum diagram.

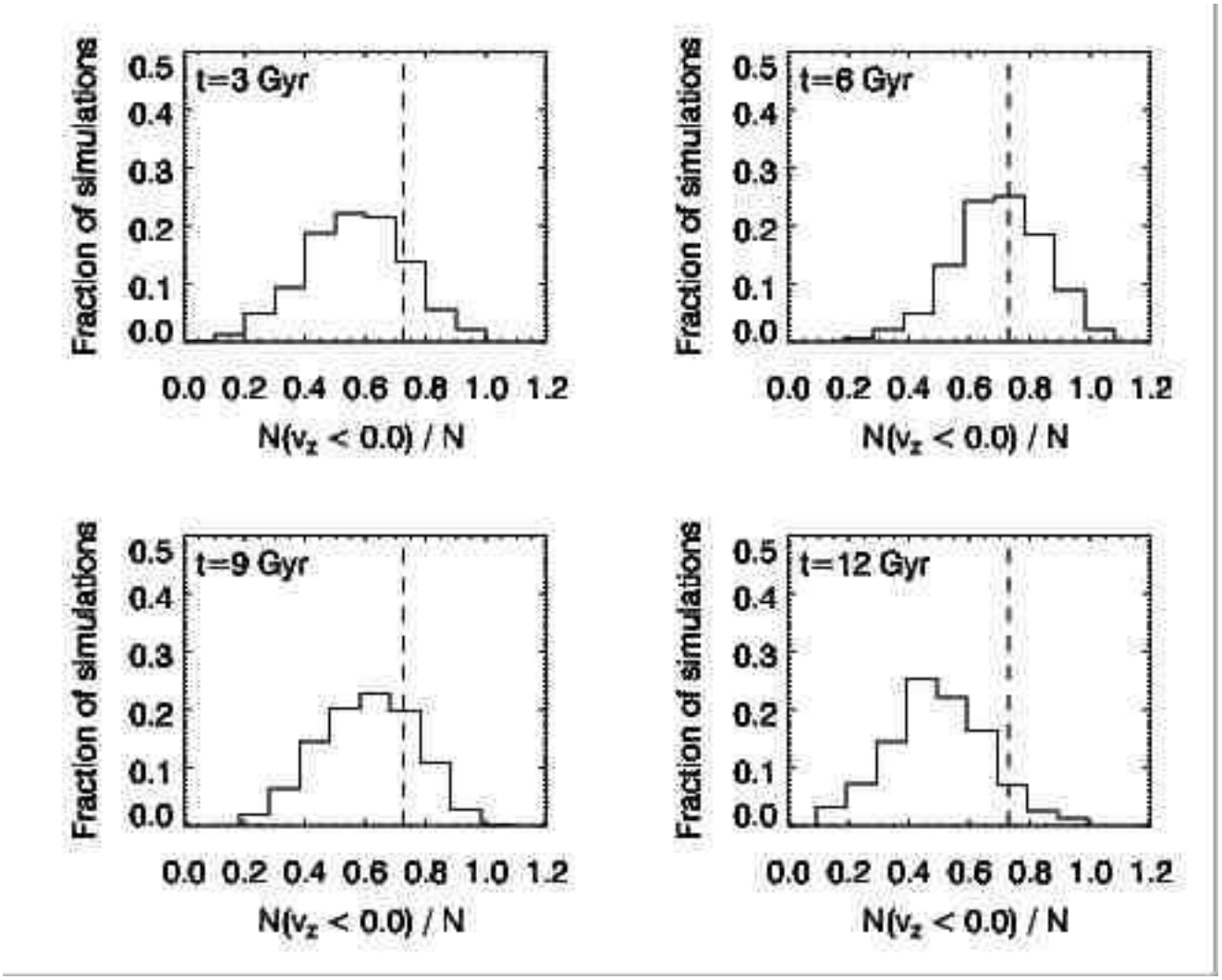


Fig. 12.— Probability that the stream with negative v_z will make up a given fraction of the total number of stars from the accreted satellite near the Sun calculated using the H99 model at four different times: 3, 6, 9, and 12 Gyr. The dashed line indicates the observed fraction of stars in this stream ($8/11 = 0.72$).



Fig. 13.— H99 model (x, y, z) and the local, Sun-centered (x', y', z') coordinate systems. Note that both the H99 model coordinate system and the local, Sun-centered coordinate system are left-handed. The direction of Galactic rotation is in the positive y'-direction.